Effects of Tetracaine on Voltage-activated Calcium Sparks in Frog Intact Skeletal Muscle Fibers

Stephen Hollingworth,[1] W. Knox Chandler,[2] and Stephen M. Baylor[1]

[1]Department of Physiology, University of Pennsylvania School of Medicine, Philadelphia, PA 19104
[2]Department of Cellular and Molecular Physiology, Yale University School of Medicine, New Haven, CT 06520

The properties of Ca^{2+} sparks in frog intact skeletal muscle fibers depolarized with 13 mM [K^+] Ringer's are well described by a computational model with a Ca^{2+} source flux of amplitude 2.5 pA (units of current) and duration 4.6 ms (18 °C; Model 2 of Baylor et al., 2002). This result, in combination with the values of single-channel Ca^{2+} current reported for ryanodine receptors (RyRs) in bilayers under physiological ion conditions, 0.5 pA (Kettlun et al., 2003) to 2 pA (Tinker et al., 1993), suggests that 1–5 RyR Ca^{2+} release channels open during a voltage-activated Ca^{2+} spark in an intact fiber. To distinguish between one and greater than one channel per spark, sparks were measured in 8 mM [K^+] Ringer's in the absence and presence of tetracaine, an inhibitor of RyR channel openings in bilayers. The most prominent effect of 75–100 μM tetracaine was an approximately sixfold reduction in spark frequency. The remaining sparks showed significant reductions in the mean values of peak amplitude, decay time constant, full duration at half maximum (FDHM), full width at half maximum (FWHM), and mass, but not in the mean value of rise time. Spark properties in tetracaine were simulated with an updated spark model that differed in minor ways from our previous model. The simulations show that (a) the properties of sparks in tetracaine are those expected if tetracaine reduces the number of active RyR Ca^{2+} channels per spark, and (b) the single-channel Ca^{2+} current of an RyR channel is ≤1.2 pA under physiological conditions. The results support the conclusion that some normal voltage-activated sparks (i.e., in the absence of tetracaine) are produced by two or more active RyR Ca^{2+} channels. The question of how the activation of multiple RyRs is coordinated is discussed.

The Journal of General Physiology

INTRODUCTION

Skeletal muscle is activated by the release of Ca^{2+} from the sarcoplasmic reticulum (SR) into the myoplasm, where it can react with the Ca^{2+} regulatory sites on troponin. This release takes place through Ca^{2+} channels in the SR called ryanodine receptors (RyRs), which are under the control of voltage sensors in the membranes of the transverse tubular system. Small, brief, localized releases through one or more of these channels can occur either spontaneously or with small depolarizations. These microscopic events, which can be detected optically with Ca^{2+} indicators, were first observed in cardiac myocytes and called Ca^{2+} sparks (Cheng et al., 1993). Because they are thought to represent the elementary event of SR Ca^{2+} release, their study is expected to lead to useful information about the release process itself.

In frog intact twitch fibers, a voltage-activated spark is thought to result from the flux of Ca^{2+} through 1–5 active release channels (18°C; Baylor et al., 2002). A goal of the present experiments was to find out whether a spark is produced by one or more than one release channel. This question was studied with tetracaine, a blocker of SR Ca^{2+} release, which has been widely used in studies of excitation–contraction coupling. In single RyR channels in bilayers, tetracaine decreased open-channel probability of both skeletal (Xu et al., 1993; Csernoch et al., 1999) and cardiac (Gyorke et al., 1997) RyRs. The drug appears to block the channel by stabilizing a closed state of the channel without a change in single channel current. The reported values of the half-inhibitory concentration of tetracaine and of the Hill coefficient vary with preparation and recording conditions: 150 μM (mean; range 75–750 μM) and 2.5, respectively, for rabbit skeletal RyRs (Xu et al., 1993); 68 μM and 1.5 for rat skeletal RyRs (Csernoch et al., 1999); and 260–650 μM and 1.9–2.2 for rat cardiac RyRs (Gyorke et al., 1997).

Several studies show that tetracaine also affects the properties of Ca^{2+} sparks. In rat ventricular myocytes, 100 μM tetracaine reduced spark frequency by a factor >5; the inhibition lasted 2–3 min after which spark frequency was approximately normal (Lukyanenko et al., 2001). This recovery was attributed to enhanced loading of the SR with Ca^{2+} in tetracaine. Also in rat ventricular myocytes, 100 μM tetracaine reduced the average rate of rise of in-focus sparks by approximately threefold without altering the ~1.2 pA quantal Ca^{2+} flux

Correspondence to Stephen M. Baylor: baylor@mail.med.upenn.edu

Abbreviations used in this paper: CICR, Ca^{2+}-induced Ca^{2+} release; FDHM, full duration at half maximum; FWHM, full width at half maximum; PSF, point-spread function; RyR, ryanodine receptor; SR, sarcoplasmic reticulum.

attributed to a single active RyR Ca^{2+} release channel (Wang et al., 2004). The latter result supports the idea that most cardiac sparks in the absence of tetracaine are produced by several simultaneously active channels.

In frog cut skeletal fibers, 200 μM tetracaine eliminated voltage-activated Ca^{2+} sparks elicited by a step depolarization from −90 to −58 mV (Shirokova and Rios, 1997) but spared a nonspark form of Ca^{2+} release elicited by a smaller depolarization, from −90 to −72 mV. This form of release, termed "small-event" Ca^{2+} release, is thought to arise from Ca^{2+} fluxes that are smaller than those that produce sparks. Shirokova and Rios (1997) hypothesized that, in the absence of tetracaine, small-event release is a voltage-controlled source of Ca^{2+} that, at larger depolarizations, is able to activate a cluster of RyRs via Ca^{2+}-induced Ca^{2+} release (CICR), thereby triggering a spark (see also Gonzalez et al., 2000).

In the present study, we have measured the effects of tetracaine on the properties of voltage-activated Ca^{2+} sparks in frog intact skeletal muscle fibers microinjected with fluo-3 (Minta et al., 1989) and depolarized by 8 mM $[K^+]$. This value of $[K^+]$ was chosen because it produces a substantial number of sparks while causing a minimal increase in resting fluorescence. The concentration of tetracaine, 75–100 μM, was selected to block most sparks but leave enough for reliable measurements. The most obvious effect of 75–100 μM tetracaine was an approximately sixfold reduction in spark frequency. Although spark rise time was unchanged, tetracaine significantly reduced the mean values of other spark morphological parameters: peak amplitude, decay time constant, FDHM, FWHM, and spark mass. These effects of tetracaine are well simulated by our spark model (updated in this study) under the assumption that tetracaine substantially reduces the amplitude of the Ca^{2+} source flux without changing its duration. This suggests that normal sparks in intact frog fibers are produced by more than one active SR Ca^{2+} release channel. To our knowledge, this is the first demonstration of a pharmacological agent other than Mg^{2+} (Gonzalez et al., 2000) that is able to reduce but not eliminate the source flux of voltage-activated sparks in skeletal muscle fibers.

In addition, in fibers in 8 or 12.5 mM $[K^+]$ Ringer's, 200 μM tetracaine essentially eliminated sparks and reduced the resting fluorescence of fluo-3 to values similar to that measured in normal Ringer's ($[K^+]$ = 2.5 mM) without tetracaine. This result differs from that reported in frog cut fibers, in which small depolarizations were found to elicit a nonspark form of SR Ca^{2+} release, as assessed by an increase in fluo-3 fluorescence, that was not blocked by 200 μM tetracaine (Shirokova and Rios, 1997).

Preliminary versions of the results and of the updated model have been presented in abstract form (Hollingworth et al., 2005; Chandler et al., 2006).

MATERIALS AND METHODS

Spark Experiments

The experimental methods were similar to those of Hollingworth et al. (2001). Microinjections of intact single fibers of *Rana pipiens* were performed on an optical bench apparatus (Baylor and Oetliker, 1977) with a membrane-impermeant form of the fluorescent Ca^{2+} indicator fluo-3 (K_5fluo-3; Molecular Probes Inc.). The spatially averaged fluorescence signal from fluo-3 was measured in this apparatus in response to an action potential (16°C). A fiber was accepted for study if $\Delta F/F_R$, the change in the indicator's fluorescence intensity divided by its resting fluorescence intensity, was ≥15. For the seven fibers that were used for the principal spark measurements of this study, the mean value of $\Delta F/F_R$ was 27.7 ± 0.5 (mean ± SEM). The mean value measured at the end of the experiment was 16.1 ± 2.1.

To measure sparks, an injected fiber was transferred to a recording chamber mounted on a home-built laser-scanning confocal microscope operating in line-scan mode (18°C). The sarcomere length of the fiber was set to ∼3.0 μm (range, 2.8–3.1 μm, determined from confocal images). The values of FWHM of the microscope point-spread function (PSF), measured with 0.1 μm fluorescent beads, are 0.21 μm in x and y and 0.51 μm in z. x-t fluorescence intensity images (F(x,t)) were recorded from fiber regions that contained ∼0.1 mM fluo-3. The laser intensities used to excite fluo-3 were about twice those used previously (Hollingworth et al., 2001). This increased the fluorescence signal–noise ratio so that smaller sparks could be detected (see below). The values of F_R, which were measured by a pair of photon-counting avalanche photodiodes, were typically 5–7 counts per μs in the present study compared with 2–4 counts per μs in the previous study. In those experiments, the standard deviation of $\Delta F/F_R$ in the nonspark regions of the unsmoothed images was typically ∼0.26, whereas in the present experiments, it was ∼0.17.

Three different solutions were used in most spark experiments. Recording began in normal Ringer's solution (NR), which contained (in mM) 120 NaCl, 2.5 KCl, 1.8 $CaCl_2$, 5 PIPES (pH 7.1). This solution was then changed to an elevated $[K^+]$ Ringer's (8–12.5 mM $[K^+]$, made by the addition of K_2SO_4 to NR); this depolarized the fibers and stimulated sparks. The expected value of membrane potential in 8 mM $[K^+]$ Ringer's (8K Ringer's) is about −70 mV and, in 12.5 mM $[K^+]$ Ringer's (12.5K Ringer's), about −60 mV (Hodgkin and Horowicz, 1959). The solution was then changed to elevated $[K^+]$ Ringer's containing tetracaine (made by addition of tetracaine hydrochloride; Sigma-Aldrich). In most experiments, $[K^+]$ was 8 mM and the concentration of tetracaine was 75–100 μM. With this concentration of tetracaine, the frequency of sparks in 8K Ringer's was reduced but not eliminated, and a sufficient number of sparks could be recorded in tetracaine to permit useful statistical comparisons between spark properties in the absence and presence of the drug. To bracket the effects of the solution changes, sparks were then measured in elevated $[K^+]$ Ringer's without tetracaine and, finally, in NR. After each solution change, the fiber was allowed to stabilize for 4 min before confocal recording was resumed. Typical times in the solutions were 10–15 min for each exposure to NR, 20–25 min for each exposure to elevated $[K^+]$ Ringer's without tetracaine, and 30–60 min for exposure to elevated $[K^+]$ Ringer's with tetracaine.

Optical Bench Experiments

Other experiments were performed in the optical bench apparatus to determine F_R in different solutions (described in Figs. 7 and 8 in RESULTS). As in the spark experiments, an intact single fiber was microinjected with fluo-3, and the fiber was accepted for study if $\Delta F/F_R$ in response to an action potential was ≥15. Spatially averaged (nonconfocal) values of F_R were measured from a 300 μm length of fiber centered at the injection site using

the methods described by Harkins et al. (1993). The measurements were performed with fibers bathed in NR and in 8 and 12.5K Ringer's, both with and without tetracaine (16°C; sarcomere length = 3.24 ± 0.10 μm, n = 12). The optical bench experiments typically lasted 2–3 h, similar to the spark experiments on the confocal microscope. The mean ± SEM values of $\Delta F/F_R$ in response to an action potential measured at the beginning and end of these experiments were 22.8 ± 1.4 and 20.1 ± 0.9, respectively (n = 12).

Analysis of Sparks

The raw F(x,t) images were converted to $\Delta F/F_R$ images, in which F_R here denotes the average intensity at any x of image pixels not containing sparks. Sparks were identified in 3 × 3 smoothed $\Delta F/F_R$ images by an automatic detection program. The increased laser intensities (see above) allowed the detection threshold of $\Delta F/F_R$ to be set at 0.2, rather than 0.3 as used previously (Hollingworth et al., 2001), with the result that smaller sparks could be detected. Checks with the method described in Hollingworth et al. (2001) showed that, with a detection threshold of 0.2, false sparks were <1% of detected sparks in the present experiments. Similarly, false sparks were <1% in simulations performed to mimic these conditions (described below).

The morphological parameters of detected sparks were determined from fits of standard functions (Eqs. 1 and 2 of Hollingworth et al., 2001) to spark profiles in time and space extracted from unsmoothed $\Delta F/F_R$ images (illustrated in RESULTS). A spark was accepted if its morphological parameters satisfied the following criteria: fitted peak $\Delta F/F_R \geq 0.5$ (unless noted otherwise); 0–100% rise time, 1–12 ms; decay time constant, 0–15 ms; FDHM, 2.5–15 ms; FWHM, 0.3–3 μm. These criteria differ slightly from those described in Hollingworth et al. (2001): fitted peak $\Delta F/F_R \geq 0.7$; 0–100% rise time, 0.4–25 ms; decay time constant, 0–20 ms; FDHM, 2.5–40 ms; FWHM, 0.3–4 μm.

Prior to the selection of sparks with fitted peak ≥ 0.5, the values of $\Delta F/F_R$ in solutions other than NR were scaled (multiplied) by the ratio F_T/F_{NR}, in which F_T and F_{NR} denote values of F_R in the test solution and NR, respectively. This scaling of amplitudes corrects for changes in F_R caused by changes in resting $[Ca^{2+}]$ ($[Ca^{2+}]_R$) associated with the solution changes. Thus, after scaling, spark amplitudes in the test solutions are referred to those expected in NR.

Two methods were used to estimate F_T/F_{NR}. In the first method, F_T/F_{NR} was estimated in each spark experiment from the ratio of values of F_R measured on the confocal microscope in closely adjacent fiber regions shortly before and shortly after each solution change (Hollingworth et al., 2001). The second method used results from fibers studied in the optical bench apparatus, with F_T/F_{NR} obtained from the average values of F_R measured in different test solutions relative to that in NR. With the first method, the mean values of F_T/F_{NR} and the number of fibers (n) used for the measurements were 1.205 for 8K Ringer's without tetracaine (n = 8) and 1.064 for 8K Ringer's with 75–100 μM tetracaine (n = 7). With the second method, the values were 1.144 for 8K Ringer's without tetracaine (n = 12) and 1.023 for 8K Ringer's with 80 μM tetracaine (n = 3). Thus, both methods gave similar values of F_T/F_{NR}, which are not very different from 1.0. The second method was used for the F_T/F_{NR} corrections in RESULTS.

The effect of the F_T/F_{NR} correction factor was evaluated in two spark simulations with a Ca^{2+} source flux of 1.7 pA for 4.2 ms (the same values used in column 6 of Table III). One had $[Ca^{2+}]_R$ = 50 nM to give F_T/F_{NR} = 1.0 and the other had $[Ca^{2+}]_R$ = 59.08 nM to give F_T/F_{NR} = 1.144, as was used in the experiments. For each simulation, 200,000 noisy sparks were generated and analyzed using the procedures described below except that the amplitude of the sparks with $[Ca^{2+}]_R$ = 59.08 nM was multiplied by 1.144. The corresponding mean values of the primary morphological factors (rise time, peak $\Delta F/F_R$, decay time constant, FDHM, and FWHM) differed by <1%; the derived morphological parameter spark mass (=1.206× peak $\Delta F/F_R$ × FWHM^3; Hollingworth et al., 2001) differed by 6.5%. These differences are small compared with the effects of tetracaine on spark morphological properties described in RESULTS.

Spark Model 3

Ca^{2+} sparks were modeled using the general procedures of Baylor et al. (2002). A spark is assumed to be driven by a brief flux of Ca^{2+} that enters the myoplasm at a point source. Ca^{2+} then spreads by diffusion while binding to both fluo-3 and the intrinsic Ca^{2+} buffers of myoplasm. The source flux is assumed to have a fixed amplitude and duration. In most simulations, resting myoplasmic free $[Ca^{2+}]$ ($[Ca^{2+}]_R$) was assumed to be 50 nM, consistent with estimates from intact fibers of *R. pipiens* in NR (Hollingworth et al., 2001).

The set of reaction–diffusion equations and the values of the associated reaction rate constants and diffusion coefficients (collectively termed Model 3) differed in several ways from those used previously (Model 2; Baylor et al., 2002). As described below, spark simulations with both models were found to produce similar estimates of the amplitude and duration of the Ca^{2+} source flux and of the mean values of the spark morphological parameters. Greater differences, however, were found in simulations of large SR Ca^{2+} release events, such as that elicited by an action potential (Fig. 2, described below). Model 3 is thought to represent myoplasmic conditions more accurately than Model 2 and was used for the spark simulations in this article. The differences between Models 2 and 3, and the reason for each modification, are given below.

1. The Kinetics of the Ca^{2+}–Troponin Reaction. In spark Model 1 (Baylor et al., 2002), a simple one-step reaction was used to simulate the binding of Ca^{2+} to each of the two regulatory sites on troponin; the same forward and reverse reaction rate constants were used for both sites (18°C; 1.017×10^8 $M^{-1}s^{-1}$ and 132 s^{-1}, respectively; dissociation constant = 1.3 μM). With Model 1, the falling phase of simulated sparks failed to match that of measured sparks.

In Model 2, a two-step reaction was used for Ca^{2+} binding to troponin (Fig. 1 A; see also Baylor et al. 2002). The forward rate constant from Model 1 was used for each site but different values were used for the reverse rate constants. These were chosen rather arbitrarily as 20 × 132.1 = 2,642 s^{-1} and 132.1/20 = 6.6 s^{-1}, depending on whether troponin had one or two bound Ca^{2+} ions, respectively. This multiplication and division by the same factor leaves the geometric mean of the two dissociation constants unchanged, 1.3 μM; hence the value of free $[Ca^{2+}]$ at which half the regulatory sites are bound with Ca^{2+} is unchanged, 1.3 μM. The properties of sparks simulated with Model 2 agreed well with the measured properties.

In Model 3, the same two-step reaction is used except that the values of k_{-1} and k_{-2} from Model 2 were divided and multiplied, respectively, by 1.49. This makes the rate constant of Ca^{2+} dissociation from troponin agree with that measured experimentally, as described in the next paragraph. Values of troponin's rate constants in Model 3 are given in part A of Table I; the forward rate constant of the first reaction and the reverse rate constant of the second reaction are twice those of each site because two Ca^{2+}-free sites are available for the first forward reaction and two Ca^{2+}-bound sites are available for the second reverse reaction. Because the values of k_{+1} and k_{+2} are the same as those in Model 2, the values of the Ca^{2+} dissociation constants (column 4 in part A of Table I) are 1.49-fold smaller and larger, respectively, than those in Model 2; the geometric mean of the dissociation constants is unchanged, 1.3 μM.

TABLE I

Rate Constants Assumed in Spark Model 3 for the Reactions Shown in Fig. 1 (18°C)

	1	2	3	4
	Reaction	Forward rate	Reverse rate	Ratio
A	$Ca^{2+} + Trop \leftrightharpoons TropCa$	$2.033 \times 10^8\ M^{-1}s^{-1}$	$1{,}771\ s^{-1}$	8.72 μM
	$Ca^{2+} + CaTrop \leftrightharpoons TropCa_2$	$1.017 \times 10^8\ M^{-1}s^{-1}$	$19.7\ 0\ s^{-1}$	0.194 μM
B	$Ca^{2+} + E \leftrightharpoons ECa$	$10^8\ M^{-1}s^{-1}$	$4\ s^{-1}$	0.04 μM
	$Ca^{2+} + ECa \leftrightharpoons ECa_2$	$10^8\ M^{-1}s^{-1}$	$5\ s^{-1}$	0.05 μM
	$Mg^{2+} + E \leftrightharpoons EMg$	$10^5\ M^{-1}s^{-1}$	$5\ s^{-1}$	50 μM
	$Mg^{2+} + EMg \leftrightharpoons EMg_2$	$10^5\ M^{-1}s^{-1}$	$100\ s^{-1}$	1,000 μM
	$H^+ + E \leftrightharpoons EH$	instantaneous	instantaneous	pK = 8
	$H^+ + EH \leftrightharpoons EH_2$	instantaneous	instantaneous	pK = 8
	$H^+ + EH_2 \leftrightharpoons EH_3$	instantaneous	instantaneous	pK = 6
	$H^+ + EH_3 \leftrightharpoons EH_4$	instantaneous	instantaneous	pK = 5
	$ECa_2 \leftrightharpoons E + (2Ca^{2+})$	$4\ s^{-1}$	0	0

Parts A and B give parameters for the reactions in Fig. 1 (A and B) (troponin and the SR Ca^{2+} pump, respectively). Forward (column 2) and reverse (column 3) rate constants are denoted by k_{+i} and k_{-i} (i = 1, 2, etc.), respectively. Column 4 gives the dissociation constant ($=k_{-i}/k_{+i}$) for each reaction involving Ca^{2+}, Mg^{2+}, or protons; the dissociation constant of the proton reactions are expressed as pKs (in parentheses). The parentheses on the right-hand side of the last reaction in column 1 of part B denote the two Ca^{2+} ions that are released into the lumen of the SR as a result of the transport step of the pump. At the resting values of $[Ca^{2+}]$, $[Mg^{2+}]$, and pH in the model (50 nM, 1 mM, and 7, respectively), the resting fractional occupancies of the different states in the reaction schemes are: 0.9928, 0.0057, and 0.0015 for Trop, TropCa, and $TropCa_2$, respectively; and 0.0062, 0.0039, 0.0008, 0.1236, 0.1236, 0.0618, 0.6179, 0.0618, and 0.0006 for E, ECa, ECa_2, EMg, EMg_2, EH, EH_2, EH_3, and EH_4, respectively.

The selection of the new value of k_{-2} in Model 3 is based on the experimental findings of Davis et al. (2004). These authors measured the apparent rate at which Ca^{2+} dissociates from troponin on reconstituted thin filaments of rabbit muscle; this rate is expected to essentially equal k_{-2} since $k_{-1} >> k_{-2}$. The measured value was 16 s^{-1} at 15°C; this corresponds to 19.7 s^{-1} at 18°C if a Q_{10} of 2 is assumed. The value of k_{-2} was changed from 13.21 s^{-1} in Model 2 to 19.7 s^{-1} in Model 3 ($=1.49 \times 13.21\ s^{-1}$) so that the apparent rate of Ca^{2+} dissociation from troponin would match the value of Davis et al.; the value of k_{-1} was adjusted to keep the value of the geometric mean of the dissociation constants unchanged.

2. Ca^{2+} Binding and Transport by the SR Ca^{2+} Pump. Fig. 1 B shows the multistep reaction used in Model 3 to simulate the binding and transport of Ca^{2+} by the SR Ca^{2+} pump. The binding steps are taken from the ion binding scheme of Peinelt and Apell (2002); the Ca^{2+} transport step (indicated by the arrow from ECa_2 to E, with rate constant k_{+9}) was not included in Peinelt and Apell (2002) but is used here to describe the translocation of Ca^{2+} into the SR lumen. Possible translocation of Mg^{2+} and/or H^+ is not considered here. The binding steps involve competition among H^+, Mg^{2+}, and Ca^{2+} for the transport sites. Because Peinelt and Apell (2002) gave only dissociation constants for the binding reactions (column 4 in Table I B), kinetic calculations require that either a forward or reverse rate constant be chosen for each reaction step. Forward rate constants were selected; the values for Ca^{2+} and Mg^{2+} are similar to those often used for reactions between these cations and proteins ($10^8\ M^{-1}s^{-1}$ for Ca^{2+}; $10^5\ M^{-1}s^{-1}$ for Mg^{2+}; column 2 of Table I B). Each reverse rate constant (column 3) was then calculated from the product of the forward rate constant and the dissociation constant. Because the reactions of protein sites with H^+ are expected to be much more rapid than those with Ca^{2+} and Mg^{2+}, we assume that the reactions between H^+ and their binding sites are in equilibrium. The value of k_{+9} (4 s^{-1}) was chosen to satisfy two criteria (Young et al., 2003): (1) R_{max}, the steady-state turnover rate of the pump at saturating $[Ca^{2+}]$, should be several per second at 18°C, and (2) $Ca_{1/2}$, the value of free $[Ca^{2+}]$ at which steady-state turnover equals half R_{max}, should be in the low micromolar range. With $k_{+9} = 4\ s^{-1}$ (column 2 in Table I B), both conditions are satisfied: $R_{max} = 3.96\ s^{-1}$ and $Ca_{1/2} = 3.41$ μM. With a total enzyme concentration of 0.12 mM (Baylor et al., 1983, 2002), the maximal rate of Ca^{2+} translocation is 0.95 mM Ca^{2+} ions s^{-1} ($= 3.96\ s^{-1} \times 0.12$ mM $\times$ 2).

The reaction scheme for the Ca^{2+} pump in Fig. 1 B has a major advantage over that used in spark Model 2 (Baylor et al., 2002); it requires only ~0.7 times as much Ca^{2+} to be released from the SR to simulate the Ca^{2+} transient elicited by an action potential. This advantage arises because the new scheme uses competitive binding of nontransportable ions, which decreases the number of pump sites immediately available to bind Ca^{2+}. Otherwise, with similar concentrations of transport and troponin regulatory sites, as occurs in frog muscle, and similar forward rate constants for Ca^{2+} binding, both types of sites would be expected to bind Ca^{2+} at similar rates.

Fig. 2 shows two single-compartment simulations that illustrate the differences between Model 2 (A) and Model 3 (B). The lowermost traces show the change in myoplasmic free $[Ca^{2+}]$ (denoted by $\Delta[Ca^{2+}]$) estimated for a single myofibril of a frog twitch fiber in response to an action potential. Also shown are (a) the calculated changes in concentration of Ca^{2+} bound to the principal Ca^{2+} buffer sites of myoplasm: ATP, troponin, parvalbumin, and the SR Ca^{2+} pump (changes with respect to resting values denoted by $\Delta[CaATP]$, $\Delta[CaTrop]$, $\Delta[CaParv]$, $\Delta[CaPump]$, respectively), (b) the change in total myoplasmic Ca^{2+} concentration ($\Delta[Ca_T]$, calculated as the sum of the five lower traces), and (c) the rate of change of $\Delta[Ca_T]$ (labeled "Release"), which estimates the flux of Ca^{2+} into the myoplasm through the SR Ca^{2+} release channels. The $\Delta[CaPump]$ traces show that much less Ca^{2+} is bound to the pump in Model 3 than in Model 2. At 8 ms, which is approximately the time of peak of the $\Delta[CaTrop]$ traces, the value of $\Delta[CaPump]$ in Fig. 2 B is <10% that in Fig. 2 A, 11.8 and 146.6 μM, respectively (or 11.6 and 137.8 μM if pump translocation of Ca^{2+} is ignored). As a consequence, the maximum values of the $\Delta[Ca_T]$ and Release traces are smaller in Model 3 than in Model 2: 387 and 560 μM for $\Delta[Ca_T]$ and 200 and 244 μM/ms for Release. The $\Delta[CaTrop]$ traces show that the rate of rise and the rate of fall of $\Delta[CaTrop]$ are both slightly faster in Model 3 than in Model 2; however, the peak value of $\Delta[CaTrop]$ is very similar in the two models, 232 and 230 μM, respectively.

In extreme cases, such as superfast twitch fibers of the toadfish swimbladder, the concentration of Ca^{2+} pump molecules appears to be several times that of the troponin regulatory sites (Appelt et al., 1991). In these fibers, the Ca^{2+} required to bind to the pump sites in the absence of competitive binding of nontransportable ions is calculated to be several times that required to bind to the troponin regulatory sites, and the advantage of competitive binding is expected to be even larger (Hollingworth and Baylor, 1996).

3. The Free Diffusion Coefficient of Fluo-3 in Myoplasm. In Model 3, the value assumed for the free diffusion coefficient of fluo-3 in myoplasm is slightly smaller than that in Model 2: 1.42 and 1.510^{-6} cm^2s^{-1}, respectively. This change was made to provide a more accurate temperature correction for fluo-3's diffusion coefficient at 18°C.

4. The Myoplasmic Concentration of Protein Sites that Are Available To Bind Fluo-3. Most Ca^{2+} indicators, including fluo-3 (Harkins et al., 1993), bind strongly to relatively immobile

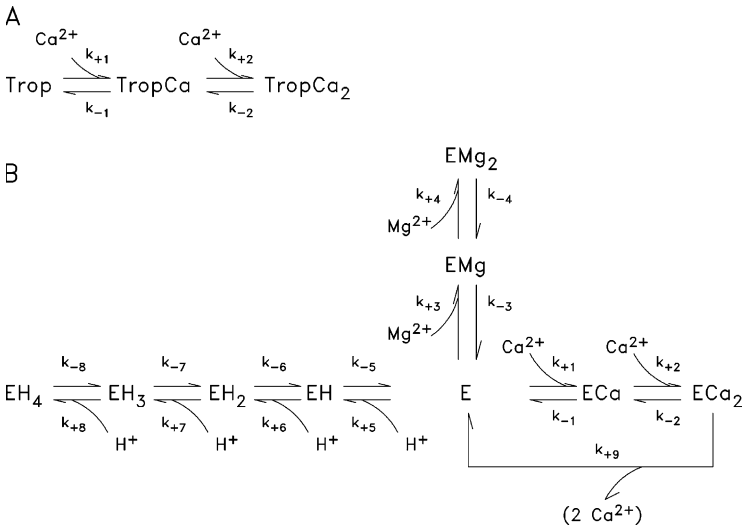

Figure 1. Model 3 reaction schemes for the troponin regulatory sites (A) and the SR Ca^{2+} pump (B); in B, the protein moiety of the pump is denoted by E. The values of the rate constants and dissociation constants of the reaction steps are given in Table I; the total myoplasmic concentration of both troponin and pump molecules is 120 μM. The reaction schemes and rate constants for the other myoplasmic constituents in the model (ATP, parvalbumin, fluo-3, and protein) are the same as in Baylor et al. (2002).

myoplasmic constituents such as soluble and structural proteins (Zhao et al., 1996). This property of fluo-3 is incorporated into Model 2 with a reaction scheme in which both Ca^{2+}-free and Ca^{2+}-bound indicator can bind to immobile myoplasmic sites, denoted by Pr. In Model 2, the concentration of immobile sites, 3 mM, gave f = 0.88, where f is the fraction of fluo-3 bound to Pr in a resting fiber. This value of f is consistent with the value of fluo-3′s apparent diffusion coefficient, D_{app}, measured previously in resting fibers, $0.20 \pm 0.02 \times 10^{-6}$ cm^2s^{-1} (Harkins et al., 1993) and the assumption that D_{app} and D, the free myoplasmic diffusion coefficient, are related by the equation: $D_{app} = D(1 - f)$ (Maylie et al., 1987).

In Model 3, the value of [Pr] has been reduced from 3 to 1 mM. This reduces the fraction of fluo-3 molecules bound to Pr and increases D_{app}, consistent with our recent measurements. In these experiments, performed in the optical bench apparatus, the measured value of D_{app} was $0.47 \pm 0.04 \times 10^{-6}$ cm^2s^{-1} ($n = 4$), which is 2–2.5 times larger than the previously reported value, $0.20 \pm 0.02 \times 10^{-6}$ cm^2s^{-1}. This larger value seems appropriate for modeling our Ca^{2+} sparks because fiber conditions were similar in the recent measurements of D_{app} and in the spark experiments. Peak $\Delta F/F_R$ of fluo-3 in response to an action potential was 26.9 ± 1.4 at the start of the D_{app} measurements and 22.2 ± 1.4 at the end (measured, on average, 126 min later). These values are similar to those measured in the spark experiments of this study, 27.7 ± 0.5 at the start and 16.1 ± 2.1 at the end (see above) as well as those in the spark experiments of Hollingworth et al. (2001). In contrast, peak $\Delta F/F_R$ in the experiments of Harkins et al. (1993) was considerably smaller, 6.8 ± 0.5. This smaller value

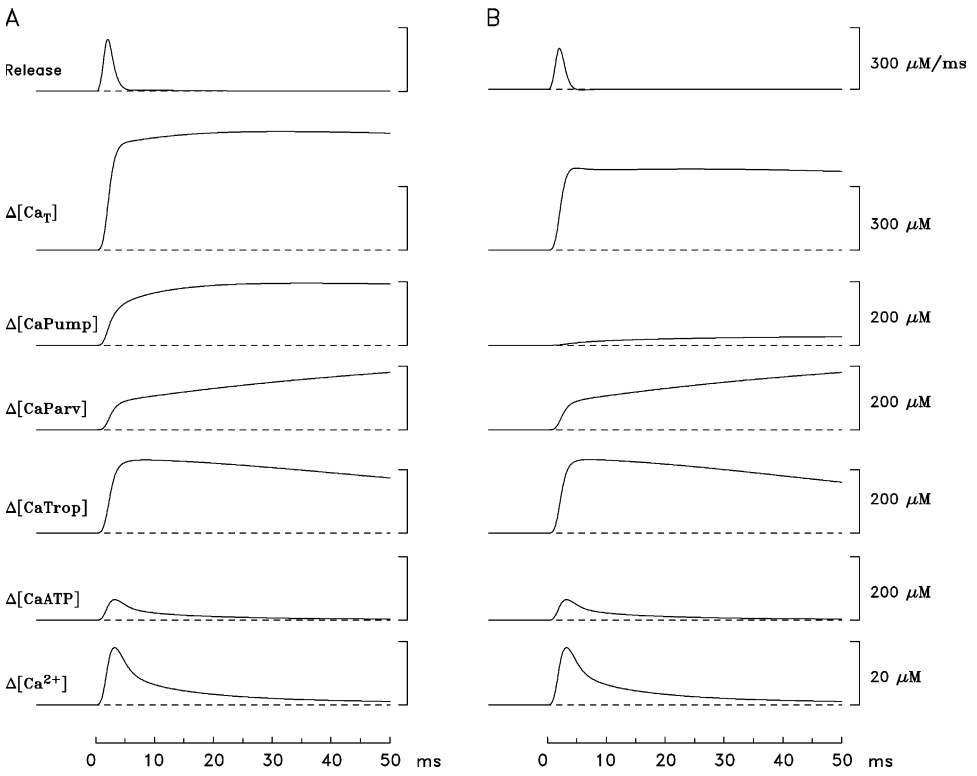

Figure 2. Simulated changes in Ca^{2+} binding to the major myoplasmic Ca^{2+} buffers elicited by an action potential. The reactions in Models 2 and 3 were used for A and B, respectively. In both panels, the bottom trace shows spatially averaged free $\Delta[Ca^{2+}]$ (from Fig. 4 of Baylor and Hollingworth, 1998); this was used in single-compartment calculations to obtain changes in the four Ca^{2+} buffers shown above each $\Delta[Ca^{2+}]$ trace. The trace labeled $\Delta[Ca_T]$ is the sum of the five lower traces; the trace labeled Release is $(d/dt)\Delta[Ca_T]$. Each Δ[CaPump] trace includes an almost negligible contribution from Ca^{2+} ions translocated into the SR.

TABLE II

Comparison of Measured and Simulated Sparks in 12.5K Ringer's (18°C; peak $\Delta F/F_R \geq 0.7$)

1	2	3	4
Parameter and units	Measurements	Model 2 2.5 pA × 4.6 ms	Model 3 2.4 pA × 5.0 ms
Distance (μm)	–	0.405 ± 0.003	0.451 ± 0.003
0-100% rise time (ms)	4.176 ± 0.034	4.194 ± 0.023	4.168 ± 0.025
Peak amplitude ($\Delta F/F_R$)	1.082 ± 0.007	1.077 ± 0.005	1.089 ± 0.006
Decay time constant (ms)	4.601 ± 0.044	5.747 ± 0.037	3.753 ± 0.032
FDHM (ms)	5.923 ± 0.037	6.820 ± 0.030	5.314 ± 0.024
FWHM (μm)	1.019 ± 0.007	1.014 ± 0.005	1.075 ± 0.006
Mass (μm³)	1.938 ± 0.047	1.528 ± 0.027	1.996 ± 0.034

Mass = 1.206 × peak $\Delta F/F_R$ × FWHM³ (Hollingworth et al., 2001). Columns 2–4 show mean ± SEM values of morphological parameters obtained from fits to 3,176 individual sparks that used $\Delta F/F_R$ values of 0.3 for detection threshold and ≥0.7 for fitted peak $\Delta F/F_R$ (column 2, measured sparks; columns 3 and 4, sparks simulated with Models 2 and 3, respectively, with 0.26 for the standard deviation of the added noise). The differences between the simulations in columns 3 and 4 are described in the text. Row 1 gives the distance between the scan line and the spark source in the y-z plane, which is known in the simulations (distance = $\sqrt{(y^2 + z^2)}$) but not in the measurements. The numbers at the top of columns 3 and 4 are the amplitude and duration of the Ca^{2+} source flux used in the simulations.

is thought to reflect a larger value of $[Ca^{2+}]_R$ and consequently a larger value of F_R (for a given concentration of indicator) in the fibers of Harkins et al. (1993).

The likely explanation of the smaller D_{app} in the earlier experiments is that the fluo-3 injections in those experiments produced some minor damage; as a result, membrane depolarization near the injection site could slow the diffusion of fluo-3, whose charge is −5, away from the injection site. The larger $[Ca^{2+}]_R$ estimated in those fibers probably also reflects minor damage. Interestingly, in one fiber in our recent experiments, results similar to those found by Harkins et al. (1993) were obtained: $\Delta F/F_R$ was 6.7 at the start of the experiment and 9.5 at the end (measured 125 min later), and the measured value of D_{app} was 0.21×10^{-6} cm² s⁻¹. Since this value of $\Delta F/F_R$ is below our current criterion for acceptability, no other results are reported for this fiber.

With [Pr] reduced to 1 mM in Model 3, the new value of f at $[Ca^{2+}]_R$ = 50 nM is 0.7, which is consistent with $D_{app} = 0.47 \times 10^{-6}$ cm² s⁻¹.

Simulation of Noisy Sparks and Estimation of their Morphological Parameters

The procedure for estimating the Ca^{2+} flux that produces a spark was the same as that described by Baylor et al. (2002). The first step was to make initial guesses of the flux amplitude and duration. Concentrations of free $[Ca^{2+}]$ and its buffers were then calculated at different times after the onset of the Ca^{2+} flux and at different distances from the point source of release. The fluorescence of fluo-3 was spatially filtered with a PSF that approximated that of the experimental apparatus to give $\Delta F/F_R$. A random number generator was used to simulate the main sources of noise and variability that contribute to the $\Delta F/F_R$ measurements. These include instrumentation and photon noise (predominantly photon noise), random displacement of the scan line relative to the spark source, and random spark onset relative to the time of data sampling. The simulation of photon noise was changed slightly from that described by Baylor et al. (2002). In those simulations, random noise of mean zero and constant standard deviation (SD) was added to each pixel of the simulated $\Delta F/F_R$ image. Because photon noise is expected to be proportional to $\sqrt{F}$, in this article the noise in each pixel was multiplied by $\sqrt{(1+\Delta F/F_R)}$. The value of SD was set equal to the average standard deviation of the noise in the nonspark region of measured images. The smaller value of SD in the present measurements, 0.17 (vs. 0.26 in Hollingworth et al. 2001), reflects the larger signal–noise ratio of $\Delta F/F_R$.

A large number of simulated noisy sparks (either 200,000 or sufficient to give the same number as the experiment) were generated with their Ca^{2+} source at the center of the y-z plane and with the scan line intersecting the plane randomly within a square 2.05 μm × 2.05 μm centered at the origin. These were analyzed exactly like measured sparks, including use of the same $\Delta F/F_R$ threshold for spark detection and the same criteria for spark acceptance. The entire procedure was then repeated with new estimates of source flux amplitude and duration until the simulated mean values of spark rise time and peak $\Delta F/F_R$ matched those of the measurements.

Spark Simulations with Model 3 Are Similar to Those with Model 2

The preceding three sections describe the changes in the methods of analysis and simulations used in this article. Table II shows properties of measured sparks and sparks simulated with the previous Model 2 and the new Model 3. Column 2 shows the mean ± SEM values of the principal morphological parameters of sparks in 12.5K Ringer's described by Hollingworth et al. (2001; also given in column 2 of Table V of Baylor et al., 2002). These were obtained from fits to 3,176 individual sparks that satisfied peak $\Delta F/F_R \geq 0.7$. Column 3, which was taken from column 3 of Table V of Baylor et al. (2002), shows simulation results with Model 2 for the same number of sparks. These simulations used an SD for added noise of 0.26, a $\Delta F/F_R$ detection threshold of 0.3, and a fitted peak $\Delta F/F_R$ criterion of ≥0.7. Column 4 shows analogous results with Model 3 with the same values of SD, detection threshold, and fitted peak $\Delta F/F_R$ criterion. The values of flux amplitude and duration estimated in the two simulations (Table II, top of columns 3 and 4) agree within 10%. Model 2 does a better job of simulating the measured FWHM, whereas Model 3 does a better job of simulating spark mass and a slightly better job of simulating FDHM. In both simulations, the parameter that is least well simulated is the decay time constant; Model 2 overestimates the value by 25% whereas Model 3 underestimates the value by 23%. On balance, both simulations appear to produce reasonable overall agreement with the measurements.

Statistics

The statistical significance of a difference between means was evaluated with Student's two-tailed *t* test; results were considered significant if $P < 0.01$. *t* tests were performed with MLAB (Civilized Software, Inc.)

RESULTS

Effects of 75–100 μM Tetracaine on Ca^{2+} Sparks

Fig. 3 shows spark frequency vs. time during one of seven experiments that evaluated the effect of tetracaine on the properties of Ca^{2+} sparks elicited by 8K Ringer's. The sequence of solutions (indicated at the top) was NR, 8K Ringer's, 8K Ringer's with 80 μM tetracaine, 8K Ringer's, and NR. The frequencies of sparks with fitted peak $\Delta F/F_R \geq 0.5$ are given in the legend. The average values in each solution were (in sarcomere⁻¹s⁻¹): 0.030 in NR, 0.212 in 8K Ringer's without tetracaine,

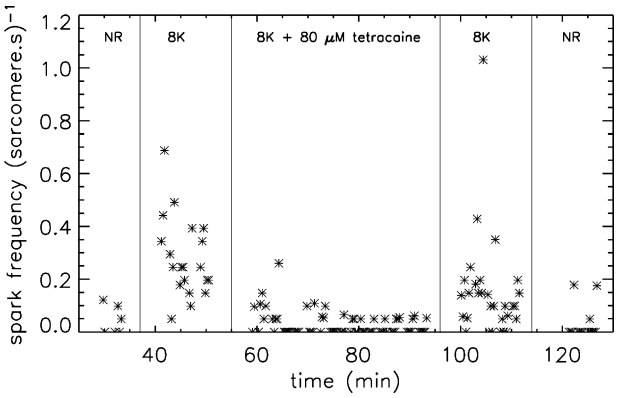

Figure 3. Spark frequency (ordinate) vs. time (abscissa) for a fiber in NR, 8K Ringer's without tetracaine, 8K Ringer's with 80 μM tetracaine, 8K Ringer's without tetracaine, and NR. Each asterisk shows the frequency of sparks with peak $\Delta F/F_R \geq 0.5$ in one 1.6-s x-t image. The average frequencies (in sarcomere^{-1}s^{-1}) in the five solutions were: 0.042, 0.280, 0.027, 0.145, and 0.018, respectively. Fiber number, z090204b.

and 0.027 in 8K Ringer's with 80 μM tetracaine. Thus, in this experiment, 8K Ringer's increased spark frequency by a factor of ~7 (relative to NR), and 80 μM tetracaine decreased spark frequency in 8K Ringer's by a factor of ~8. These frequencies are similar to those observed in the seven experiments of this type. The mean ± SEM values were (in sarcomere^{-1}s^{-1}): 0.027 ± 0.009 in NR, 0.184 ± 0.041 in 8K Ringer's without tetracaine, and 0.032 ± 0.008 in 8K Ringer's with 75–100 μM tetracaine.

The frequency of sparks remained fairly constant during exposure to tetracaine. In the seven experiments described above, the frequencies during the first and last 10 min in tetracaine were 0.039 ± 0.012 and 0.024 ± 0.007 sarcomere^{-1}s^{-1}, respectively; these values are not significantly different. This result in frog skeletal muscle contrasts with that in rat ventricular myocytes where spark frequency in tetracaine recovered after an initial inhibition (see DISCUSSION).

Fig. 4 shows sample x-t images recorded while the fiber was in 8K Ringer's (lefthand panels, without tetracaine; righthand panels, with tetracaine). The upper images are displayed in raw fluorescence intensity units, whereas the lower images are in $\Delta F/F_R$ units. Several sparks can be seen in each image. As expected, these sparks are centered on z-lines (see legend).

The top panels in Fig. 5 show zoomed $\Delta F/F_R$ images of the two sparks marked by arrowheads in Fig. 4. The asterisks in the middle and bottom panels show the spark profiles in time and space, respectively; the curves show fits of the standard empirical functions. From the fits, estimates were obtained for the values of rise time, peak $\Delta F/F_R$, decay time constant, FDHM, FWHM, late baseline offset, and spark mass (see legend and values printed on figures).

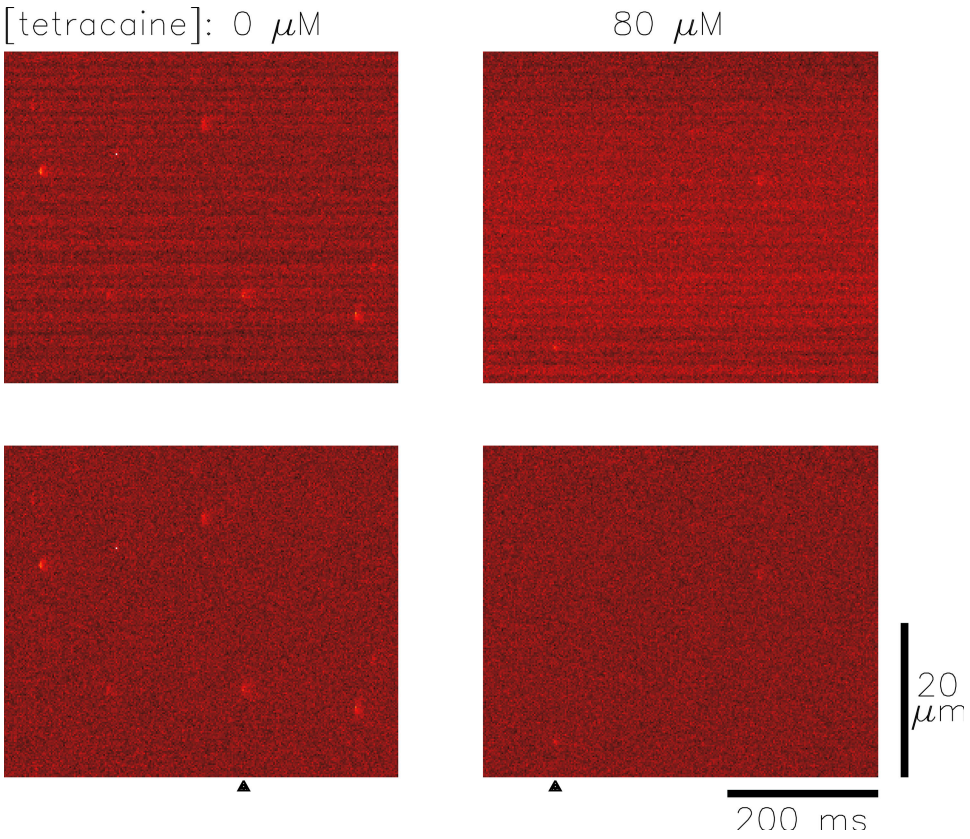

Figure 4. Fluorescence images from a fiber in 8K Ringer's exposed to 0 and 80 μM tetracaine (left and right panels, respectively). Top, raw x-t images. The sarcomere length of the fiber, 3.1 μm, was calculated from the spatial periodicity in F, in which the thinner and thicker fluorescent bands are centered on m-lines and z-lines, respectively (Hollingworth et al., 2001). Several Ca^{2+} sparks are visible in each image; they occur at z-lines. Bottom, same data after conversion to $\Delta F/F_R$. See Fig. 5 for $\Delta F/F_R$ calibrations. Same fiber as in Fig. 3

Columns 2–5 of Table III give the number of sparks and the mean values (± SEM) of their frequency and morphological parameters determined in the seven tetracaine experiments described above. The second row gives frequency in absolute units; the third row gives frequency relative to that in 8K Ringer's without tetracaine. Columns 2 and 3 give values in 8K Ringer's before and after tetracaine, respectively; column 4 gives values from all images used for columns 2 and 3. Column 5 gives similar information for 8K Ringer's with 75–100 μM tetracaine. The reduction in frequency to 0.176 ± 0.022 times that in 8K Ringer's without tetracaine is significantly different from 1.0 ($P < 0.01$).

Columns 2 and 3 of Table III show that the values of the spark morphological parameters (last six rows) are similar for the first and second exposures to 8K Ringer's. The only parameter that is significantly different is spark rise time, 3.53 ± 0.06 and 3.82 ± 0.07 ms, respectively ($P < 0.01$); the percentage difference is small, however, 8%. Columns 4 and 5 show that all morphological parameters, with the exception of rise time, are reduced significantly in tetracaine ($P < 0.01$). The mean percentage reductions are 11% for peak $\Delta F/F_R$, 19% for decay time constant, 11% for FDHM, 9% for FWHM, and 29% for spark mass. Thus, 75–100 μM tetracaine clearly alters the morphological parameters of sparks in 8K Ringer's. Since spark rise time closely tracks the duration of the underlying Ca^{2+} source flux (e.g., Table VI of Baylor et al., 2002), especially at the Ca^{2+} source, the constancy of rise time suggests that the duration of Ca^{2+} release that produces a spark is similar with and without tetracaine. Consequently, the smaller values of peak $\Delta F/F_R$ and other morphological parameters in tetracaine suggest that the mean amplitude of the underlying Ca^{2+} source flux is reduced by tetracaine.

If a spark in 8K Ringer's without tetracaine is due to one active RyR Ca^{2+} channel and tetracaine acts simply to stabilize a closed state of the channel (Xu et al., 1993; Gyorke et al., 1997; Csernoch et al., 1999), tetracaine would be expected to reduce the frequency of sparks without changing peak $\Delta F/F_R$ or other morphological parameters. Since this is not the case, a normal voltage-activated spark in 8K Ringer's appears to require more than one active release channel. This is one of the main results of this study.

Comparison of Simulated and Measured Ca^{2+} Sparks

Model 3 was used to simulate sparks in 8K Ringer's with and without 75–100 μM tetracaine. The approach

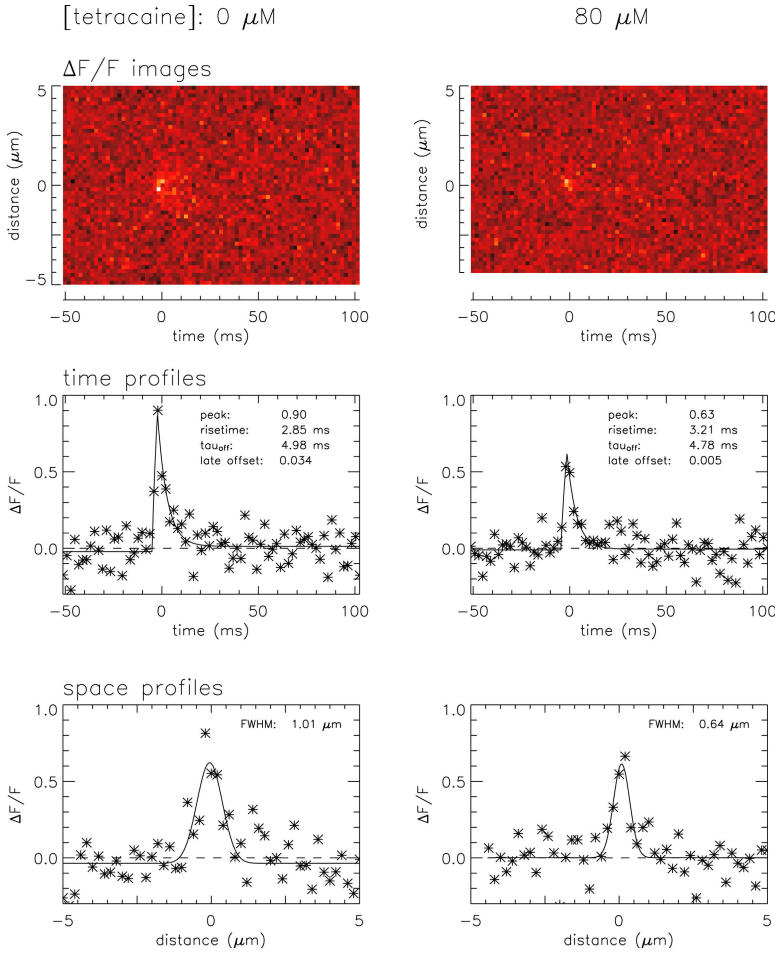

Figure 5. The top panels show zoomed $\Delta F/F_R$ images of the two sparks identified by the arrowheads in Fig. 4. In the middle panels, the asterisks show $\Delta F/F_R$ profiles in time extracted at the spatial center of each spark (average of the three time lines at −0.2, 0, and +0.2 μm from the spark center); the curve is the fit of Eq. 1 in Hollingworth et al. (2001). In the bottom panels, the asterisks show profiles in space extracted at the time of peak of each spark (average of two line scans, the ones just before and just after the fitted time of peak); the curve is a fit of a gaussian function (Eq. 2 of Hollingworth et al., 2001). The values of the morphological parameters not printed on the figure are 5.22 and 5.27 ms for FDHM (left and right, respectively) and 1.07 and 0.20 μm^3 for spark mass.

TABLE III

Effects of Tetracaine on the Frequency and Morphology of Measured and Simulated Ca^{2+} Sparks in 8K Ringer's (18°C; Peak $\Delta F/F_R \geq 0.5$)

1	2	3	4	5	6	7
Parameter and units	$[K^+]$ = 8 mM [tetracaine] = 0	$[K^+]$ = 8 mM [tetracaine] = 0	$[K^+]$ = 8 mM [tetracaine] = 0	$[K^+]$ = 8 mM [tetracaine] = 75–100 μM	Model 3 1.7 pA × 4.2 ms	Model 3 1.2 pA × 4.2 ms
Number of sparks	520	541	1,061	262	49,457	30,536
Frequency (sarcomere^{-1}s^{-1})	0.192 ± 0.047	0.177 ± 0.042	0.184 ± 0.041	0.032 ± 0.008[a]	–	–
Relative frequency	–	–	1.0	0.176 ± 0.022[a]	1.0	0.618
Distance (μm)	–	–	–	–	0.412 ±0.001	0.338 ± 0.001
0-100% rise time (ms)	3.53 ± 0.06	3.82 ± 0.07	3.67 ± 0.04	3.70 ± 0.09	3.68 ± 0.01	3.71 ± 0.01
Peak amplitude ($\Delta F/F_R$)	0.77 ± 0.01	0.76 ± 0.01	0.76 ± 0.01	0.68 ± 0.01[a]	0.76 ± 0.00	0.68 ± 0.00
Decay time constant (ms)	4.51 ± 0.10	4.46 ± 0.11	4.48 ± 0.07	3.64 ± 0.13[a]	3.65 ± 0.01	3.34 ± 0.01
FDHM (ms)	5.40 ± 0.08	5.58 ± 0.09	5.49 ± 0.06	4.89 ± 0.10[a]	4.86 ± 0.01	4.66 ± 0.01
FWHM (μm)	0.98 ± 0.02	0.99 ± 0.02	0.99 ± 0.01	0.90 ± 0.02[a]	1.03 ± 0.00	0.96 ± 0.00
Mass (μm^3)	1.15 ± 0.06	1.27 ± 0.07	1.21 ± 0.04	0.86 ± 0.07[a]	1.18 ± 0.01	0.94 ± 0.01

Columns 2–5 give mean ± SEM values of spark properties in seven experiments of the type illustrated in Figs. 3–5; two fibers were exposed to 75 μM tetracaine, three to 80 μM, and two to 100 μM (mean value, 84 μM). Columns 2 and 3 show values measured in 8K Ringer's before and after, respectively, the measurements in tetracaine (column 5); column 4 gives combined results from columns 2 and 3. The frequency values are the average of the seven values from the individual experiments, whereas the morphological parameter values are from fits to the combined population of sparks. All fibers had at least 15 sparks in 75–100 μM tetracaine with peak $\Delta F/F_R \geq 0.5$. The peak values of $\Delta F/F_R$ in columns 2–5 were obtained with the F_T/F_{NR} correction factors described in MATERIALS AND METHODS. Columns 6 and 7 show results of simulations with Model 3 with the amplitude and duration of the Ca^{2+} source flux adjusted to reproduce the values of rise time and peak $\Delta F/F_R$ in columns 4 and 5, respectively; the numbers at the top of the columns give the amplitude and duration of the Ca^{2+} source flux used in the two simulations. In each simulation, 200,000 sparks were generated randomly with the Ca^{2+} source at the center of a 2.05 μm by 2.05 μm square in the y-z plane and with the scan line in the x direction intersecting the square at random locations.
[a]Statistically significant difference between the parameter values in column 5 vs. columns 2, 3, and 4 at $P < 0.01$.

(MATERIALS AND METHODS) was to assume values of the amplitude and duration of the Ca^{2+} source flux, simulate 200,000 randomly varied noisy sparks, and then calculate the simulated mean values of peak $\Delta F/F_R$ and rise time; the large number of simulated sparks decreased the SEMs of the mean so that more accurate comparisons could be made between simulated and experimental means. The process was repeated with new values of flux amplitude and duration until the mean values of peak $\Delta F/F_R$ and rise time matched those of the experiments. The resulting Ca^{2+} source fluxes were 1.7 pA and 4.2 ms, respectively, without tetracaine and 1.2 pA and 4.2 ms with tetracaine (columns 6 and 7 of Table III). Overall, the mean values of the morphological parameters of both sets of simulated sparks are in reasonable agreement with the corresponding experimental values (columns 4 and 5). The flux amplitude without tetracaine, 1.7 pA, is smaller than that estimated with Model 3 for sparks measured previously in frog intact fibers, 2.4 pA (column 4 of Table II). Possible reasons for this difference are considered later in RESULTS.

The simulations in Table III indicate that the flux amplitude underlying a spark in tetracaine is ~0.7 times that in its absence and suggest that the Ca^{2+} flux through a single RyR Ca^{2+} channel in an intact frog fiber is ≤1.2 pA. The reductions in spark frequency and in the associated SR Ca^{2+} efflux by tetracaine might lead to increases in SR Ca^{2+} content and, as a result, in single-channel Ca^{2+} flux. In this case, the value of the Ca^{2+} flux in tetracaine should be decreased before comparison with control fluxes, and the upper limit of 1.2 pA should be reduced accordingly. Thus, if SR Ca^{2+} content is increased by tetracaine, some of the effects of tetracaine would appear to be more marked than those reported in this article.

Although the values of spark rise time are similar with and without tetracaine (3.67 ± 0.04 and 3.70 ± 0.09 ms, respectively, in columns 4 and 5 of Table III), it seemed important to consider the possibility that tetracaine slightly reduces the duration of SR Ca^{2+} release during a spark, as might be the case in cardiac RyRs (Gyorke et al., 1997). To test this idea, spark simulations were used to determine the maximal and minimal durations of Ca^{2+} source flux that are consistent with the rise times without and with tetracaine, respectively. The difference in these durations is <0.4 ms and suggests that any reduction in flux duration with tetracaine is expected to be <10%. The simulations also show that 1.2 pA remains a reasonable estimate of flux amplitude in tetracaine. (In these simulations, 3.79 ms was considered to be an upper limit of spark rise time without tetracaine, since a value >3.79 ms is not consistent [$P < 0.01$] with the observed value, 3.67 ± 0.04 ms [column 4 of Table III]. The Ca^{2+} flux duration that gives a rise time of 3.79 ms and a peak $\Delta F/F_R$ of 0.76 [also column 4 of Table III] is just less than 4.4 ms. With tetracaine, 3.47 ms was considered to be a lower limit of rise time, since a value <3.47 ms is not consistent [$P < 0.01$] with the observed value, 3.70 ± 0.09 ms [column 5 of Table III]. The Ca^{2+} flux duration that gives a rise time of 3.47 ms and a peak $\Delta F/F_R$

of 0.68 [also column 5 of Table III] is just greater than 4.0 ms. The difference between these durations gives the inequality <0.4 ms reported above.)

The overall conclusions from these simulations are that (a) tetracaine reduces the amplitude of the Ca^{2+} flux underlying sparks to ~0.7 times that in the absence of tetracaine (1.2 pA vs. 1.7 pA), and (b) the Ca^{2+} flux through a single RyR Ca^{2+} channel in an intact frog fiber is likely to be ≤1.2 pA.

Although the effects of tetracaine on spark morphological properties are adequately described by the simulations in Table III, the effect on spark frequency is not. The ratio of spark frequency with and without tetracaine (row 3 of Table III) is significantly different (larger) in the simulations, 0.618 (column 7), than in the measurements, 0.176 ± 0.022 (column 5) ($P < 0.01$). This indicates that the overall effect of tetracaine on sparks is not adequately simulated by a simple reduction in Ca^{2+} flux through active SR Ca^{2+} release channels. Nor would such a simple result be expected from bilayer experiments, where tetracaine's major action on the RyR Ca^{2+} channel appears to be a stabilization of a closed state, not a reduction in current through the open channel (Xu et al., 1993; Gyorke et al., 1997; Csernoch et al., 1999).

Tetracaine's combined effects on spark frequency and morphology are further analyzed in Fig. 6. The symbols show the effect of 75–100 μM tetracaine on mean spark morphological parameters in the seven experiments of Table III; the panels show rise time (A), peak $\Delta F/F_R$ (B), decay time constant (C), FDHM (D), FWHM (E), and spark mass (F). The values in tetracaine have been divided by those in the absence of tetracaine and plotted vs. frequency in tetracaine divided by that in the absence of tetracaine. These normalizations allow the data to be plotted without knowledge of the stoichiometry of tetracaine binding to the Ca^{2+} release channels. The squares show normalized mean values from the seven individual experiments, and the asterisks show the mean of the seven normalized means. In these experiments, the frequency of sparks in 75–100 μM tetracaine was reduced to 0.11–0.33 times normal; the mean reduction is 0.176 (column 5 of Table III).

As mentioned above, if a spark in 8K Ringer's without tetracaine is due to one active RyR Ca^{2+} channel and if tetracaine acts simply to stabilize a closed state of the channel, tetracaine would be expected to reduce spark frequency without a change in morphological parameters. This possibility is indicated by the horizontal line at 1.0 on the ordinate in the panels in Fig. 6. Although the normalized mean value of rise time (A) is not significantly different from 1.0 ($P = 0.33$; $n = 7$), the normalized values of the other parameters (B–F) are noticeably different (smaller), and these decreases are all significant ($P < 0.01$; $n = 7$). This analysis confirms the conclusion from Table III that more than one release channel is likely to be involved in the generation of a normal voltage-activated spark in 8K Ringer's.

The four curved lines in each panel of Fig. 6 are drawn from theories that assume that either two or four RyR Ca^{2+} channels are involved in normal spark generation. In each case, it is assumed that all RyR Ca^{2+} channels, voltage-gated and otherwise, have the same amplitude and duration Ca^{2+} flux and the same ability to bind tetracaine (and to bind it independently of the other channels). Derivation of the curves (described below) depends on binomial probabilities and the properties of sparks simulated with four different Ca^{2+} source fluxes (Table IV).

The last six rows of columns 2–5 of Table IV show that all simulated mean morphological parameter values are reduced progressively as the amplitude of the Ca^{2+} source flux is reduced in steps of 0.425 pA. The reduction in mean values from 1.7 to 0.425 pA (column 5 vs. 2) is small for rise time, 7%, but larger for the other morphological parameters: 25% for peak $\Delta F/F_R$, 45% for decay time constant, 28% for FDHM, 29% for FWHM, and 63% for spark mass. Row 4 shows that the reduction in mean distance from the scan line to the spark source is also large, 54%. Row 3 gives the peak value of $\Delta F/F_R$ of a noise-free spark with the scan line at the Ca^{2+} source ± 0.2 μm. The value of $\Delta F/F_R$ for 0.425 pA, 0.379 (column 5), does not satisfy peak $\Delta F/F_R \geq 0.5$; thus, the 514 simulated sparks that were detected with 0.425 pA must have had their fitted peak $\Delta F/F_R$ increased by random noise.

In Fig. 6, the simplest theory assumes that each release unit consists of two Ca^{2+} channels that function independently. The uppermost continuous curve in each panel was generated from this theory, calculated as follows. Since a normal Ca^{2+} spark in the present experiments is well simulated by a Ca^{2+} flux of 1.7 pA for 4.2 ms, a single channel is assumed to have a Ca^{2+} flux of $1.7/2 = 0.85$ pA for 4.2 ms. If f denotes the fraction of release channels blocked by tetracaine (i.e., stabilized in the closed state), then $(1 - f)^2$, $2f(1 - f)$, and f^2 are, respectively, the fraction of release units that have zero, one, and two channels blocked by tetracaine and, consequently, that can flux 1.7, 0.85, and 0 pA of Ca^{2+}. As indicated in row 2 of Table IV, the relative frequency of accepted sparks with a flux of 1.7 and 0.85 pA, is 1.0 and 0.2667, respectively. Since release units with two blocked channels do not produce sparks, $1.0 \times (1 - f)^2 + 0.2667 \times 2f(1 - f)$ gives the frequency of sparks relative to that in the absence of tetracaine; this gives the abscissa value in each panel of Fig. 6 for a particular value of f. Similarly, the corresponding value on the ordinate in each panel in Fig. 6 is the weighted average of the mean parameter values in columns 2 and 4 of Table IV, calculated with the relative weighting factors $1.0 \times (1 - f)^2$ and $0.2667 \times 2f(1 - f)$. The theoretical curves

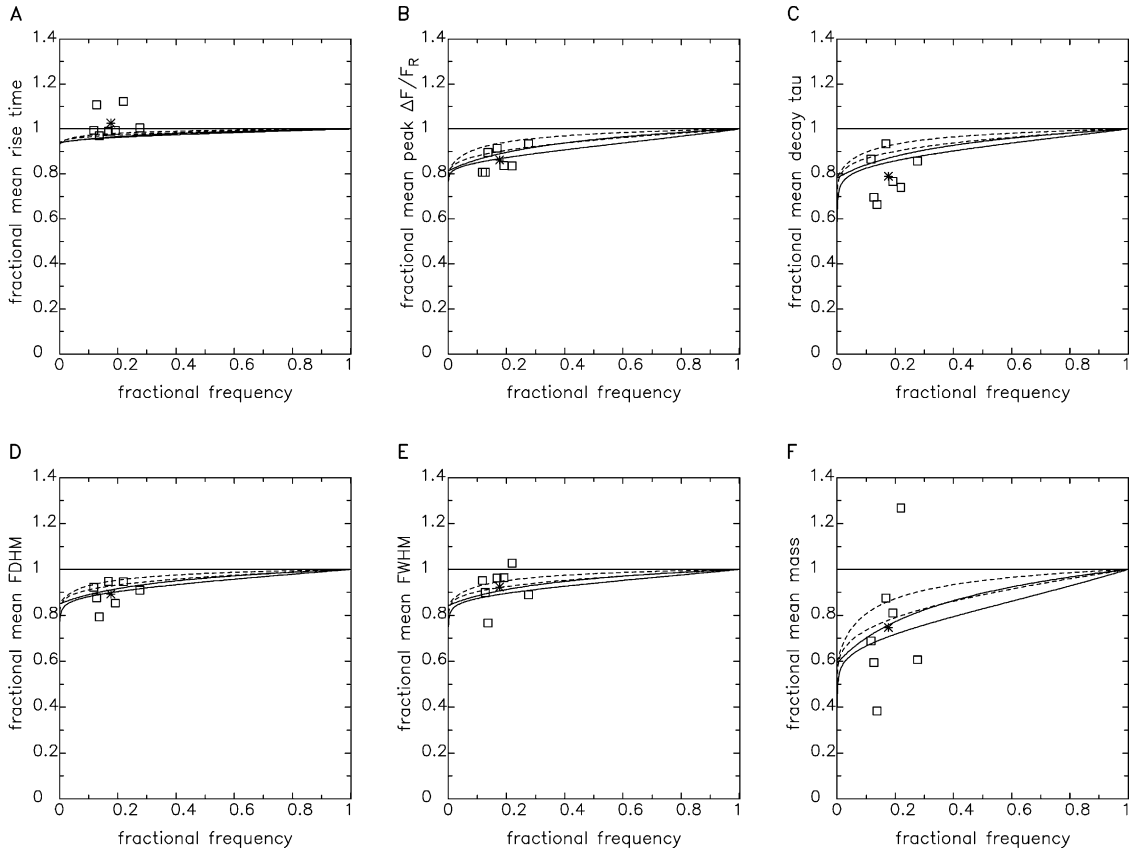

Figure 6. Effect of tetracaine on normalized spark properties. In each panel, the symbols show mean values of a particular morphological parameter with tetracaine relative to that without tetracaine plotted vs. the spark frequency with tetracaine relative to that without tetracaine (peak $\Delta F/F_R$ criterion of ≥ 0.5). The open squares show the individual means from seven experiments; the asterisks show the mean value of these means. The horizontal lines show the predictions of the hypothesis that a normal spark is caused by a single active release channel. The curves show predictions from four hypotheses about the number of release channels per spark (two or four) and the way that these release channels are controlled, independent (continuous curves) or coupled (dashed curves), as described in RESULTS. For the average relative spark frequency of the measurements with tetracaine, 0.176 (column 5 of Table III), the different models predict the following values of f (=the probability that an individual channel is blocked by tetracaine) and of the mean number of pA per spark: 0.733 and 1.20 (two-channel independent), 0.659 and 1.41 (two-channel coupled), 0.648 and 1.09 (four-channel independent), 0.565 and 1.24 (four-channel coupled).

were determined from such calculations with many values of f between 0 and 1.

The uppermost dashed curves in Fig. 6 were obtained with another two-channel model. One release channel, the controller channel, is required to be open (and therefore not be blocked by tetracaine) for the other channel, the follower, to flux Ca^{2+}. In this case, $(1 - f)^2$, $f(1 - f)$, and f represent, respectively, the fraction of release units that can flux 1.7, 0.85, and 0 pA of Ca^{2+}. Each curve was then calculated by the method described in the preceding paragraph.

The same approach was used to model release from four Ca^{2+} channels, with fluxes of 1.7, 1.275, 0.85, 0.425, and 0 pA and corresponding probability values. The lower continuous and dashed curves in each panel are analogous to the upper curves obtained for the two-channel models.

In Fig. 6, the curves from the four multichannel models reproduce the observed effects of tetracaine on spark frequency and morphological parameters. Because the curves are spaced closely together compared with the scatter in the data, none of these theories can be ruled out. The ability of these theories to adequately simulate tetracaine's effects on both spark frequency and morphological parameters contrasts with the results in column 7 of Table III, which adequately simulated the effects on morphological parameters but not on frequency.

Effect of the Peak $\Delta F/F_R$ Criterion on the Simulated Ca^{2+} Source Flux in the Absence of Tetracaine

If the Ca^{2+} source flux underlying normal sparks is stereotypical, for example, with an amplitude of 1.7 pA and a duration of 4.2 ms, the estimated flux should be independent of the value of the peak $\Delta F/F_R$ criterion. To test this idea, the confocal images used for column 4 of Table III were analyzed with three different values of the peak $\Delta F/F_R$ criterion: ≥ 0.5 (as in column 4 of Table III), ≥ 0.7, and ≥ 1.0. Columns 2, 4, and 6 of

TABLE IV

Simulations of Ca^{2+} Sparks Carried Out with Four Different Amplitudes of the Ca^{2+} Source Flux (18°C; Peak $\Delta F/F_R \geq 0.5$)

1	2	3	4	5
Parameter and units	1.7 pA × 4.2 ms	1.275 pA × 4.2 ms	0.85 pA × 4.2 ms	0.425 pA × 4.2 ms
Number of sparks	49,457	32,161	13,188	514
Relative frequency	1.0	0.6503	0.2667	0.0104
Peak amplitude at the source ($\Delta F/F_R$)	1.375	1.061	0.729	0.379
Distance (μm)	0.412 ± 0.001	0.345 ± 0.001	0.260 ± 0.001	0.188 ± 0.005
0-100% rise time (ms)	3.675 ± 0.005	3.598 ± 0.006	3.452 ± 0.010	3.414 ± 0.047
Peak amplitude ($\Delta F/F_R$)	0.762 ± 0.001	0.692 ± 0.001	0.620 ± 0.001	0.571 ± 0.003
Decay time constant (ms)	3.647 ± 0.007	3.340 ± 0.009	2.852 ± 0.013	2.009 ± 0.053
FDHM (ms)	4.859 ± 0.005	4.581 ± 0.006	4.128 ± 0.009	3.503 ± 0.030
FWHM (μm)	1.028 ± 0.001	0.959 ± 0.002	0.866 ± 0.003	0.729 ± 0.014
Mass (μm^3)	1.184 ± 0.005	0.941 ± 0.006	0.700 ± 0.010	0.434 ± 0.039

Sparks were simulated with Model 3 using a single source flux duration, 4.2 ms, as used for the simulations in Table III, and four different source flux amplitudes (indicated at the top of the columns); the flux amplitudes are in the ratio 1:0.75:0.5:0.25. In each simulation, 200,000 noisy sparks were generated as described in Table III. The second row gives the number of sparks relative to that in column 2. The third row gives the mean amplitude of each noise-free spark at the source ± 0.2 μm. The last six rows give mean ± SEM values of morphological parameters obtained from the usual fits. The mean parameter values were used to calculate the theoretical curves in Fig. 6, as described in the text.

Table V show the results. As expected, mean peak $\Delta F/F_R$ (row 5 of Table V) increases progressively with the peak $\Delta F/F_R$ criterion; referred to the value in column 2, the values in columns 4 and 6 increase by 28% and 74%, respectively. Little change (<5%), however, is observed in the values of rise time, decay time constant, FDHM, and FWHM. As expected from the increases in peak $\Delta F/F_R$, spark mass also increases (by 12% in column 4 and 36% in column 6).

Columns 3, 5, and 7 of Table V show results of simulations with Model 3 using the peak $\Delta F/F_R$ criteria from columns 2, 4, and 6, respectively. The flux duration for all three simulations was the same, 4.2 ms. For each value of the peak $\Delta F/F_R$ criterion, the flux amplitude was adjusted, as usual, to make the mean peak $\Delta F/F_R$ of the simulated sparks match that of the corresponding measurements. Interestingly, the estimated source flux amplitude increases progressively with the peak $\Delta F/F_R$ criterion: 1.7, 1.9, and 2.5 pA, respectively. With each peak $\Delta F/F_R$ criterion, reasonable overall agreement is observed between the mean parameter values of simulated and measured sparks. On the other hand, row 2 shows that the values of relative frequency do not match those of the measurements, similar to the situation observed with tetracaine in row 3 of Table III.

The finding that a larger Ca^{2+} source flux is required for a larger peak $\Delta F/F_R$ criterion suggests that multiple Ca^{2+} flux amplitudes, rather than a single amplitude, underlie sparks in 8K Ringer's. This possibility is consistent with our earlier spark data, obtained in 12.5K Ringer's, in which measured sparks were found to have greater dispersion in their morphological properties than sparks simulated with a Ca^{2+} source flux of fixed amplitude and duration (Fig. 8 in Baylor et al., 2002).

Spark Simulations with Variable Amplitudes of Ca^{2+} Source Flux

The observation that the estimated Ca^{2+} source flux depends on the peak $\Delta F/F_R$ criterion can be explained by a release unit with several RyRs; these might operate either independently or in a controller/follower configuration, as in Fig. 6, but with their activation linked probabilistically through a "coupling coefficient." In the independent model, the coupling coefficient is the probability that any RyR in the release unit is activated; in the controller/follower model, it is the probability that a follower RyR is activated if the controller is activated.

Preliminary simulations show that this kind of model with 2, 3, 4, or 8 RyRs per release unit can explain the effect of peak $\Delta F/F$ criterion on both the estimate of the Ca^{2+} source flux and the relative frequency of sparks. The SEMs of the mean values of peak $\Delta F/F_R$, however, are too large to determine the exact number of RyRs or the Ca^{2+} flux through a single RyR. Related simulations show that the effect of tetracaine on spark properties can be explained by tetracaine fully blocking one or more channels in a release unit (i.e., as considered in the models in Fig. 6) without a change in coupling coefficient. Thus, the conclusions of the analysis in Fig. 6 are not limited to the special case that sparks in the absence of tetracaine are caused by a stereotypical Ca^{2+} source flux of fixed amplitude and duration.

The Ca^{2+} Source Flux in the Absence of Tetracaine May Vary with $[K^+]$

The values of flux amplitude and duration in column 4 of Table II, 2.4 pA and 5.0 ms (standard deviation of added noise, 0.26; detection threshold, 0.3; peak $\Delta F/F_R$ criterion, ≥0.7; estimated membrane potential, −60 mV) are larger than those in column 5 of Table V, 1.9 pA and

TABLE V

Effect of Peak $\Delta F/F_R$ Criterion on Measured and Simulated Sparks in 8K Ringer's without Tetracaine (18°C)

1	2	3	4	5	6	7
Parameter and units	Measurements	Model 3	Measurements	Model 3	Measurements	Model 3
	peak $\Delta F/F_R \geq 0.5$	1.7 pA × 4.2 ms	peak $\Delta F/F_R \geq 0.7$	1.9 pA × 4.2 ms	peak $\Delta F/F_R \geq 1.0$	2.5 pA × 4.2 ms
Number of sparks	1,061	49,457	475	30,167	149	22,351
Relative frequency	1.0	1.0	0.448	0.610	0.140	0.452
Distance (μm)	–	0.412 ± 0.001	–	0.330 ± 0.001	–	0.272 ± 0.001
0–100% rise time (ms)	3.67 ± 0.04	3.68 ± 0.01	3.53 ± 0.06	3.56 ± 0.01	3.52 ± 0.12	3.50 ± 0.01
Peak amplitude ($\Delta F/F_R$)	0.76 ± 0.01	0.76 ± 0.00	0.98 ± 0.01	0.97 ± 0.00	1.32 ± 0.03	1.33 ± 0.00
Decay time constant (ms)	4.48 ± 0.07	3.65 ± 0.01	4.33 ± 0.10	3.51 ± 0.01	4.65 ± 0.16	3.49 ± 0.01
FDHM (ms)	5.49 ± 0.06	4.86 ± 0.01	5.26 ± 0.08	4.66 ± 0.01	5.48 ± 0.15	4.60 ± 0.01
FWHM (μm)	0.99 ± 0.01	1.03 ± 0.00	0.97 ± 0.01	0.97 ± 0.00	0.96 ± 0.02	0.95 ± 0.00
Mass (μm^3)	1.21 ± 0.04	1.18 ± 0.01	1.36 ± 0.06	1.19 ± 0.01	1.66 ± 0.12	1.44 ± 0.01

Columns 2 and 3 are the same as columns 4 and 6 of Table III. The recorded images used for column 2 were re-analyzed with peak $\Delta F/F_R$ criterion of ≥0.7 (column 4) and ≥1.0 (column 6). Columns 5 and 7 are similar to column 3 except that the peak $\Delta F/F_R$ criterion was ≥0.7 and ≥1.0, respectively. In all columns, the $\Delta F/F_R$ detection threshold was 0.2; in columns 3, 5, and 7, the standard deviation of the added noise was 0.17.

4.2 ms (0.17, 0.2, ≥0.7, −70 mV). These differences could be due to the difference in the standard deviation of added noise, the detection threshold, or the difference in membrane potential. To determine the influence of detection threshold and of standard deviation of added noise, the present experiments were reanalyzed using a detection threshold of 0.3 and added noise levels in the simulations of 0.17 and 0.26. The flux amplitudes (2.1 and 2.0 pA, respectively) and durations (4.2 and 4.1 ms) are also smaller than those in column 4 of Table II, 2.4 pA and 5.0 ms. This indicates that the amplitude and duration of the Ca^{2+} flux that generates voltage-activated sparks in intact fibers may be larger at −60 mV than at −70 mV. This result about flux duration is consistent with the results of Hollingworth et al. (2001), who found that the mean rise time of sparks in 12.5K Ringer's was significantly different from (larger than) that in NR: by 13% for *R. pipiens* and 17% for *R. temporaria*. A stronger effect of membrane potential on rise time was found in the experiments of Lacampagne et al. (2000) on frog cut fibers, in which a step repolarization from +40 to −90 mV reduced the mean rise time of sparks initiated near the time of repolarization by up to 50%.

It is possible that, in intact fibers, an increase in external $[K^+]$ produces a change in SR Ca^{2+} content and that this leads to the increase in spark rise time observed. This possibility, however, would not explain the effect on rise time observed by Lacampagne et al. (2000), because they used the voltage-clamp technique.

The Effect of $[K^+]$ and Tetracaine on F_R

Changes in fluo-3's resting fluorescence, F_R, caused by changes in $[Ca^{2+}]_R$ were determined in fibers injected with fluo-3 and studied in the optical bench apparatus. Fig. 7 A shows results from an experiment in which F_R was measured 30–125 min after injection, when the fiber was bathed in NR (open circles), 8K Ringer's (open squares), 8K Ringer's with 80 μM tetracaine (filled squares), and NR with 80 μM tetracaine (filled circles). The value of F_R in NR (F_{NR}) declined during the experiment as fluo-3 diffused along the fiber axis away from the injection site. The curve shows an empirical function of time, given in the legend, that was fitted to the values of F_{NR}. This curve was used to estimate F_{NR} throughout the experiment so that F_R/F_{NR} could be determined (Fig. 7 B). F_T/F_{NR} was taken to be the average value of F_R/F_{NR} during the second half of the period after a solution change, when F_R/F_{NR} appeared to reach a quasi-steady state. This was 1.176 for 8K Ringer's, 1.028 for 8K Ringer's with 80 μM tetracaine, and 0.944 for NR with 80 μM tetracaine.

Fig. 8 A shows mean ± standard deviation (SD) values of F_T/F_{NR} from 12 experiments plotted vs. $[K^+]$ at three different tetracaine concentrations (circles, 0 μM; X's, 80 μM; squares, 200 μM). In each experiment, measurements began with the fiber in NR and were bracketed by one or more returns to NR (as in Fig. 7). The average values of F_T/F_{NR} are given in the legend; some of these were used as correction factors to refer spark amplitude in test solutions to that expected in NR (MATERIALS AND METHODS). In NR without tetracaine, the filled circle ($[K^+]$ = 2.5 mM) lies, by definition, on the dashed horizontal line at 1.0. Tetracaine slightly reduced the value of F_T/F_{NR} in NR (see legend). The average value of F_T/F_{NR} in NR with ≥80 μM tetracaine, 0.97, is indicated by the dotted horizontal line in Fig. 8 A. These results suggest that (a) fibers in NR continually release a small amount of Ca^{2+} from the SR and/or have a resting influx of Ca^{2+} from the external solution, which produces a slight elevation in $[Ca^{2+}]_R$, and (b) this Ca^{2+} entry into the myoplasm is blocked by tetracaine. Although an influx of Ca^{2+} from the external solution cannot be ruled out, this is considered unlikely because, at the potentials expected in the solutions

used in these experiments (−90 to −60 mV; $[K^+]$ = 2.5 to 12.5 mM), Ca^{2+} currents are not observed (Sanchez and Stefani, 1978; Almers and Palade, 1981).

Confocal experiments show that fibers in NR have a small but detectable frequency of sparks (0.027 ± 0.009 sarcomere^{-1}s^{-1} with a peak $\Delta F/F_R$ criterion of ≥0.5, n = 7; first section of RESULTS). This observation is consistent with the idea that resting SR Ca^{2+} release occurs as sparks. This idea is supported by our results from three other fibers, in which 75–100 μM tetracaine reduced the frequency of sparks in NR by an order of magnitude, from 0.039 ± 0.005 to 0.004 ± 0.000 sarcomere^{-1}s^{-1}.

A similar interpretation applies to the measurements of F_T/F_{NR} in elevated $[K^+]$ Ringer's. 8K Ringer's without tetracaine appears to stimulate SR Ca^{2+} release; this is indicated by an elevation of F_T/F_{NR} (Fig. 8 A) and by an increase in spark frequency of approximately sevenfold (Fig. 3 and associated text). 80 μM tetracaine reduces but does not fully block this release (Fig. 8 A) and reduces the frequency of sparks without eliminating them (Table III and Fig. 6). 200 μM tetracaine reduces F_T/F_{NR} to near or below the value in NR (Fig. 8 A) and almost completely eliminates sparks. Similar results were found in 12.5K Ringer's with and without tetracaine.

Data in the different $[K^+]$ Ringer's without tetracaine are plotted in Fig. 8 B. The value of F_T/F_{NR} minus 0.97 (ordinate) varies approximately linearly with the frequency of sparks (abscissa). This result is consistent with the idea that sparks account for most of the increases in F_T/F_{NR} above 0.97 observed with $[K^+]$ = 2.5, 8, and 12.5 mM.

DISCUSSION

The experiments described in this article show that 75–100 μM tetracaine has three main effects on voltage-activated Ca^{2+} sparks in frog intact muscle fibers depolarized by 8K Ringer's: (1) an approximately sixfold reduction in spark frequency; (2) little or no modification of spark rise time; (3) 10–30% reductions in peak $\Delta F/F_R$, decay time constant, FDHM, FWHM, and mass.

To interpret these effects quantitatively, simulations of sparks were performed that included the main sources of noise and variability that are thought to contribute to the variability of measured sparks. The simulations show that the effects of 75–100 μM tetracaine are approximately those expected if tetracaine reduces the amplitude of the Ca^{2+} source flux with little or no change in its duration. In 8K Ringer's without tetracaine, the estimated flux amplitude is 1.7 pA whereas, with 75–100 μM tetracaine, it is only 1.2 pA (columns 6 and 7 of Table III; peak $\Delta F/F_R$ criterion of ≥0.5). The observed reduction in spark frequency with tetracaine (row 3 of Table III) cannot be explained, however, by a uniform reduction in source flux through all active RyR channels. This would predict a reduction in frequency of ∼38% (column 7 of Table III), which is much smaller than that observed, ∼82% (column 5). In addition, a uniform reduction in source flux would not be expected from bilayer studies (Xu et al., 1993; Gyorke et al., 1997; Csernoch et al., 1999). Rather, our results are consistent with the idea that (a) an average normal spark is generated by more than one active channel, (b) an average spark in 75–100 μM tetracaine is generated by fewer channels, and (c) 1.2 pA is an upper limit of the Ca^{2+} flux through a single RyR channel under physiological conditions.

The upper limit of 1.2 pA is consistent with the results of Kettlun et al. (2003), who studied single RyR channels in bilayers. Their estimated single-channel Ca^{2+} flux with physiological cation concentrations (150 mM $[K^+]$, 1 mM $[Mg^{2+}]$) is 0.5 pA if trans $[Ca^{2+}]$ is 1 mM and 0.8 pA if it is 2 mM (trans $[Ca^{2+}]$ corresponds to SR luminal $[Ca^{2+}]$). Based on our estimate of 1.7 pA for the Ca^{2+} source flux of a spark in 8K Ringer's without tetracaine, the single-channel values of Kettlun et al. (2003) suggest that some sparks of this type require two to four active RyR Ca^{2+} channels. Unfortunately, our results do not indicate whether the two to four channels are contiguous or distributed within a small volume determined by the PSF of the confocal microscope.

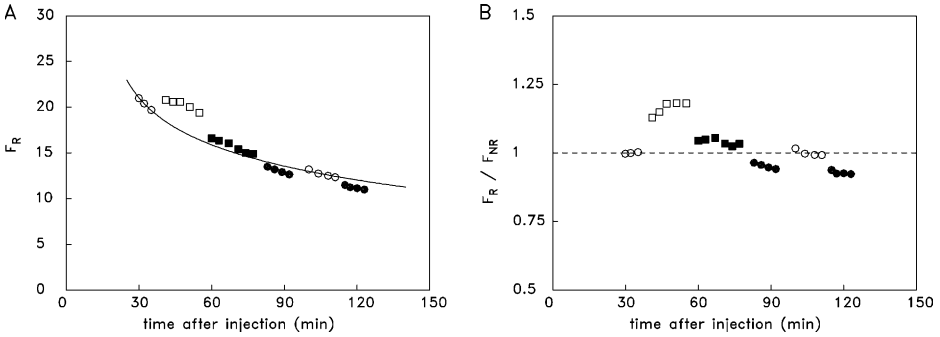

Figure 7. Fluo-3's resting fluorescence (F_R) at different times after indicator injection during exposure to four different solutions. (A) The symbols show F_R (in arbitrary units) measured in a 300-μm length of fiber, centered at the injection site, plotted against time after injection. The solution bathing the fiber was either NR (circles) or 8K Ringer's (squares) containing either 0 or 80 μM tetracaine (open and filled symbols, respectively). The curve is a plot of the empirical function $F_R(t) = k0 + k1/(t - t0)^{k2}$, which was fitted to the open circles (k0 = −131, k1 = 165.5, t0 = 15, and k2 = 0.0313). (B) Plot of F_R data from part A after normalization by F_{NR}, calculated with the empirical formula. The horizontal dashed line at 1.0 corresponds to no change in F_R relative to that in NR. Fiber number, 050205.1; sarcomere length, 2.9 μm; 16°C.

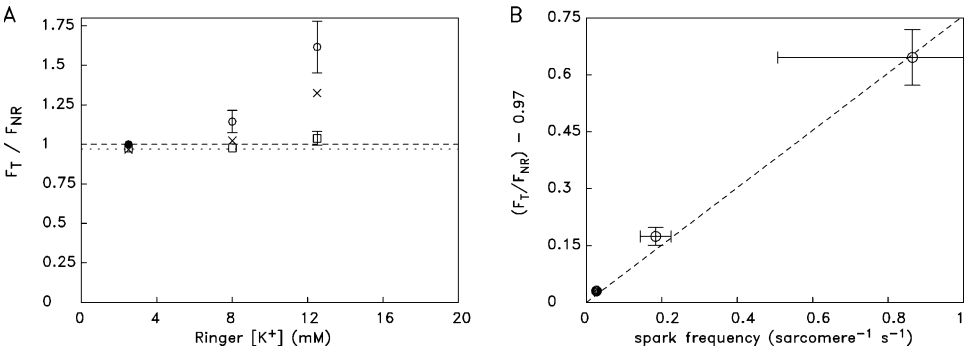

Figure 8. Dependence of F_T/F_{NR} on Ringer [K^+] and on spark frequency. (A) Mean values ±SD of F_T/F_{NR} from 12 fibers plotted vs. the [K^+] level in Ringer's (2.5, 8, and 12.5 mM) at three different concentrations of tetracaine (0 μM, circles; 80 μM, X's; 200 μM, squares). The average values on the ordinate and the number of experiments (n) that contributed to the averages in 0, 80, and 200 μM tetracaine are: 1.0 (12), 0.9665 (3), and 0.9751 (3), respectively, in 2.5 mM [K^+]; 1.1440 (9), 1.0233 (3), and 0.9780 (2) in 8 mM [K^+]; 1.6157 (5), 1.3241 (3), and 1.0376 (3) in 12.5 mM [K^+]. For the measurements in which SD exceeded the symbol size, vertical wings extend one SD above and below the mean. The dashed line at 1.0 corresponds to no change with respect to NR. The dotted line at 0.97 corresponds to the expected value of F_T/F_{NR} in the absence of SR Ca^{2+} release (see text). (B) Mean values of $F_T/F_{NR} - 0.97$ from part A plotted vs. spark frequency measured in the absence of tetracaine at the three values of [K^+]: 2.5 mM ($F_T/F_{NR} = 1.0$; number of sparks $N = 79$ from 7 fibers), 8 mM ($F_T/F_{NR} = 1.144$; $N = 1{,}061$ from 7 fibers), and 12.5 mM ($F_T/F_{NR} = 1.616$; $N = 1{,}306$ from 3 fibers); peak $\Delta F/F_R$ criterion of ≥0.5. The ordinate value of the filled circle (2.5 mM [K^+]) is, by definition, 0.03. The frequency of sparks in 12.5K Ringer's may be underestimated because of the relatively large value of F_T/F_{NR} in 12.5K Ringer's, 1.616, that was used to correct spark amplitudes. For the measurements in which SEM exceeded the symbol size, vertical and horizontal wings extend one SEM about the mean. The dashed curve is a least-squares fit to the mean values of a straight line constrained to intersect the origin.

Possible Mechanisms of RyR Coupling

The conclusion that some sparks require activation of two to four RyR channels leads to the question of how the opening of multiple RyRs is coordinated. Lacampagne et al. (1999) showed that RyR coupling must be very rapid. They studied voltage-activated sparks in frog cut fibers with rapid (63 μs) data sampling and found that $\Delta F/F_R$ rises abruptly from baseline and declines abruptly from peak, with the maximal rates of rise and decline reached shortly after the times of the respective transitions. Thus, the RyR Ca^{2+} channels appear to open and close in near synchrony.

Two mechanisms have been suggested to explain the coordinated opening of a cluster of RyR channels: (1) local protein–protein interaction(s) between adjacent RyRs (e.g., "coupled gating;" Marx et al., 1998) and (2) diffusional activation of RyRs by Ca^{2+} ions (Ca^{2+}-induced Ca^{2+} release; Endo et al., 1970; Ford and Podolsky, 1970; Rios and Pizarro, 1988). In either case, activation of the first RyR in a cluster would be initiated by its voltage sensor in the T-tubular membrane.

The coordinated closing of the cluster probably depends on Ca^{2+} inactivation of Ca^{2+} release (Baylor et al., 1983; Schneider and Simon, 1988) and/or a change in the voltage sensor.

Block of Ca^{2+} Release by Tetracaine

As described in INTRODUCTION, Shirokova and Rios (1997) found that, in frog cut fibers, 200 μM tetracaine blocked voltage-activated Ca^{2+} sparks but spared a non-spark form of Ca^{2+} release observed with small depolarizations ("small event" Ca^{2+} release). We also found that tetracaine reduces the frequency of voltage-activated sparks (Table III and Fig. 6), although we failed to find a tetracaine-insensitive form of Ca^{2+} release. In both 8K Ringer's (estimated membrane potential, −70 mV) and in 12.5K Ringer's (estimated membrane potential, −60 mV), 200 μM tetracaine reduced F_T/F_{NR} to a value near that in NR (Fig. 8 A). The simplest hypothesis to explain these results is that in intact fibers, there is one form of SR Ca^{2+} release, with an elementary release event that can be detected as sparks, and that this release is blocked by tetracaine.

Comparison with Results in Cardiac Myocytes

In our experiments, sparks were measured for up to 1 h in 8K Ringer's with 75–100 μM tetracaine. During this time, spark frequency was about sixfold smaller than that in 8K Ringer's without tetracaine (0.032 vs. 0.184 sarcomere^{-1}s^{-1}; Table III) and showed no sign of recovery (Fig. 3 and first section of RESULTS). This result differs markedly from that in rat cardiac myocytes, in which tetracaine's effect on spark frequency was transient (Lukyanenko et al., 2001): after a 1-min exposure to 100 μM tetracaine, spark frequency was about sixfold smaller than normal but during the next 2–4 min, it recovered fully. This recovery was attributed to an increase in SR luminal [Ca^{2+}] due to continued pumping of Ca^{2+} by the SR Ca^{2+} pump while RyR Ca^{2+} channels were inhibited by tetracaine. Although tetracaine might also increase luminal [Ca^{2+}] in frog intact fibers, our conclusion that a normal spark is due to more than one RyR Ca^{2+} channel would not be altered since an elevation in luminal [Ca^{2+}] would be expected to increase the RyR single-channel Ca^{2+} flux (e.g., Kettlun et al., 2003).

As noted in the first section of DISCUSSION, the estimated single-channel RyR Ca^{2+} flux is ≤1.2 pA in a frog skeletal fiber exposed to 8K Ringer's with 75–100 μM

tetracaine. This value is consistent with the single-channel value estimated by Wang et al. (2004) for rat cardiac myocytes, 1.2 pA.

Comparison with Results in Frog Permeabilized Fibers

In a study of spontaneous Ca^{2+} sparks in frog permeabilized fibers, Shtifman et al. (2000) used Imperatoxin A, an activator of RyR Ca^{2+} channels, to estimate the number of active RyR channels per spark. Their result, one to four, is similar to that estimated in this study for voltage-activated sparks in intact fibers in 8K Ringer's, two to four (first section of DISCUSSION). The Ca^{2+} source flux of a normal spark, however, is estimated to be 8–27 pA in frog cut or permeabilized fibers (Rios et al., 1999; Chandler et al., 2003) but only 1.7–2.5 pA in frog intact fibers (Baylor et al., 2002; Table V, this study). Thus, Shtifman et al.'s estimate of one to four channels per spark in permeabilized fibers implies a single-channel Ca^{2+} flux of $\geq$2 pA, whereas our estimate of two to four channels in intact fibers implies a flux of $\leq$1.25 pA, which is consistent with the value 1.2 pA listed in column 7 of Table III. Chandler et al. (2003) noted that the larger source flux in cut or permeabilized fibers could be caused by a larger number of active release channels per spark and/or a larger single-channel Ca^{2+} flux. Shtifman et al.'s results support a contribution from a larger single-channel Ca^{2+} flux. One factor that may contribute to this is a larger value of $[Ca^{2+}]_R$, which might stimulate the SR Ca^{2+} pump and elevate SR luminal free $[Ca^{2+}]$ (Chandler et al., 2003).

In another study of spontaneous sparks in frog permeabilized fibers, Zhang et al. (2005) used azumolene, an SR Ca^{2+} release inhibitor that is similar to dantrolene. Azumolene (and dantrolene) is expected to inhibit Ca^{2+} release through both types of RyRs found in frog muscle, RyRα and RyRβ (which are analogous to the RyR1 and RyR3 isoforms, respectively, found in mammalian skeletal muscle) (Zhao et al., 2001). Azumolene reduced spark frequency to zero in a dose-dependent manner (EC_{50} of 0.25 μM, Hill coefficient of 1.44) without affecting spark morphological properties (rise time, peak amplitude, FDHM, FWHM, and spark mass). The action of azumolene was attributed to its ability to stabilize a closed state of the RyR Ca^{2+} release channel (Zhang et al., 2005). This effect of azumolene, to decrease spark frequency without affecting morphological parameters, suggests that azumolene, unlike tetracaine, blocks the Ca^{2+} source flux of a spark either completely or not at all (see first two sections of RESULTS). Although this could occur if the source were a single RyR Ca^{2+} channel, such a source seems unlikely since the Ca^{2+} current through a single RyR channel in a frog permeabilized fiber would be predicted to be $\geq$8 pA (see previous paragraph). Hopefully, additional experiments will clarify the differences between the blocking actions of azumolene and tetracaine.

This work was supported by a grant from the U.S. National Institutes of Health to S.M. Baylor (NS 17620) and W.K. Chandler (AM 37643).

Olaf S. Andersen served as editor.

Submitted: 20 December 2005
Accepted: 6 February 2006

REFERENCES

Almers, W., and P.T. Palade. 1981. Slow calcium and potassium currents across frog muscle membrane: measurements with a vaseline-gap technique. *J. Physiol.* 312:159–176.

Appelt, D., V. Shen, and C. Franzini-Armstrong. 1991. Quantitation of Ca ATPase, feet and mitochondria in superfast muscle fibres from the toadfish, *Opsanus tau*. *J. Muscle Res. Cell Motil.* 12:543–552.

Baylor, S.M., and H. Oetliker. 1977. A large birefringence signal preceding contraction in single twitch fibres of the frog. *J. Physiol.* 264:141–162.

Baylor, S.M., and S. Hollingworth. 1998. Model of sarcomeric Ca^{2+} movements, including ATP Ca^{2+} binding and diffusion, during activation of frog skeletal muscle. *J. Gen. Physiol.* 112:297–316.

Baylor, S.M., W.K. Chandler, and M.W. Marshall. 1983. Sarcoplasmic reticulum calcium release in frog skeletal muscle fibres estimated from arsenazo III calcium transients. *J. Physiol.* 344:625–666.

Baylor, S.M., S. Hollingworth, and W.K. Chandler. 2002. Comparison of modeled and measured calcium sparks in intact skeletal muscle fibers of the frog. *J. Gen. Physiol.* 120:349–368.

Chandler, W.K., S. Hollingworth, and S.M. Baylor. 2003. Simulation of calcium sparks in frog cut skeletal muscle fibers. *J. Gen. Physiol.* 121:311–324.

Chandler, W.K., S. Hollingworth, and S.M. Baylor. 2006. H and Mg binding to the Ca-transport sites of the sarcoplasmic reticulum (SR) Ca pump improves efficiency of SR Ca cycling during activation of skeletal muscle fibers. *Biophys. J.* 90:67a.

Cheng, H., W.J. Lederer, and M.B. Cannell. 1993. Calcium sparks: elementary events underlying excitation-contraction coupling in heart muscle. *Science.* 262:740–745.

Csernoch, L., P. Szentesi, S. Sarkozi, C. Szegedi, I. Jona, and L. Kovacs. 1999. Effects of tetracaine on sarcoplasmic reticulum calcium release in mammalian skeletal muscle fibres. *J. Physiol.* 515:843–857.

Davis, J.P., S.B. Tikunova, D.R. Swartz, and J.A. Rall. 2004. Measurement of Ca^{2+} dissociation rates from troponin C (TnC) in skeletal myofibrils. *Biophys. J.* 86:218a.

Endo, M., M. Tanaka, and Y. Ogawa. 1970. Calcium induced release of calcium from the sarcoplasmic reticulum of skinned skeletal muscle fibers. *Nature.* 228:34–36.

Ford, L.E., and R.J. Podolsky. 1970. Regenerative calcium release within muscle cells. *Science.* 167:58–59.

Gonzalez, A., W.G. Kirsch, N. Shirokova, G. Pizarro, M.D. Stern, and E. Ríos. 2000. The spark and its ember: separately gated local components of Ca^{2+} release in skeletal muscle. *J. Gen. Physiol.* 115:139–157.

Gyorke, S., V. Lukyanenko, and I. Gyorke. 1997. Dual effects of tetracaine on spontaneous calcium release in rat ventricular myocytes. *J. Physiol.* 500:297–309.

Harkins, A.B., N. Kurebayashi, and S.M. Baylor. 1993. Resting myoplasmic free calcium in frog skeletal muscle fibers estimated with fluo-3. *Biophys. J.* 65:865–881.

Hodgkin, A.L., and P. Horowicz. 1959. The influence of potassium and chloride ions on the membrane potential of single muscle fibres. *J. Physiol.* 148:127–160.

Hollingworth, S., and S.M. Baylor. 1996. Sarcoplasmic reticulum (SR) calcium release in intact superfast toadfish swimbladder (tsb) and fast frog twitch muscle fibers. *Biophys. J.* 70:A235.

Hollingworth, S., J. Peet, W.K. Chandler, and S.M. Baylor. 2001. Calcium sparks in intact skeletal muscle fibers of the frog. *J. Gen. Physiol.* 118:653–678.

Hollingworth, S., W.K. Chandler, and S.M. Baylor. 2005. Biophysical Society. 2376 (Abstr.).

Kettlun, C., A. Gonzalez, E. Ríos, and M. Fill. 2003. Unitary Ca^{2+} current through mammalian cardiac and amphibian skeletal muscle ryanodine receptor channels under near-physiological ionic conditions. *J. Gen. Physiol.* 122:407–417.

Lukyanenko, V., S. Viatchenko-Karpinski, A. Smirnov, T.F. Wiesner, and S. Gyorke. 2001. Dynamic regulation of sarcoplasmic reticulum Ca^{2+} content and release by luminal Ca^{2+}-sensitive leak in rat ventricular myocytes. *Biophys. J.* 81:785–798.

Lacampagne, A., C.W. Ward, M.G. Klein, and M.F. Schneider. 1999. Time course of individual Ca^{2+} sparks in frog skeletal muscle recorded at high time resolution. *J. Gen. Physiol.* 113:187–198.

Lacampagne, A., M.G. Klein, C.W. Ward, and M.F. Schneider. 2000. Two mechanisms for termination of individual Ca^{2+} sparks in skeletal muscle. *Proc. Natl. Acad. Sci. USA.* 97:7823–7828.

Marx, S.O., K. Ondrias, and A.R. Marks. 1998. Coupled gating between individual skeletal muscle Ca^{2+} release channels (ryanodine receptors). *Science.* 281:818–821.

Maylie, J., M. Irving, N.L. Sizto, and W.K. Chandler. 1987. Calcium signals recorded from cut frog twitch fibers containing antipyrylazo III. *J. Gen. Physiol.* 89:83–143.

Minta, A., J.P.Y. Kao, and R.Y. Tsien. 1989. Fluorescent indicators for cytosolic calcium based on rhodamine and fluorescein chromophores. *J. Biol. Chem.* 264:8171–8178.

Peinelt, C., and H.-J. Apell. 2002. Kinetics of the Ca^{2+}, H^{+}, and Mg^{2+} interaction with the ion-binding sites of the SR Ca-ATPase. *Biophys. J.* 82:170–181.

Rios, E., and G. Pizarro. 1988. Voltage sensors and calcium channels of excitation-contraction coupling. *News Physiol. Sci.* 3:223–227.

Rios, E., M.D. Stern, A. Gonzalez, G. Pizarro, and N. Shirokova. 1999. Calcium release flux underlying Ca^{2+} sparks of frog skeletal muscle. *J. Gen. Physiol.* 114:31–48.

Sanchez, J.A., and E. Stefani. 1978. Inward calcium current in twitch muscle fibres of the frog. *J. Physiol.* 283:197–209.

Schneider, M.F., and B.J. Simon. 1988. Inactivation of calcium release from the sarcoplasmic reticulum in frog skeletal muscle. *J. Physiol.* 405:727–745.

Shirokova, N., and E. Rios. 1997. Small event Ca^{2+} release: a probable precursor of Ca^{2+} sparks in frog skeletal muscle. *J. Physiol.* 502:3–11.

Shtifman, A., C.W. Ward, J. Wang, H.H. Valdivia, and M.F. Schneider. 2000. Effects of Imperatoxin A on local sarcoplasmic reticulum Ca^{2+} release in frog skeletal muscle. *Biophys. J.* 79:814–827.

Tinker, A., A.R.G. Lindsay, and A.J. Williams. 1993. Cation conduction in the calcium release channel of the cardiac sarcoplasmic reticulum under physiological and pathophysiological conditions. *Cardiovasc. Res.* 27:1820–1825.

Wang, S.Q., M.D. Stern, E. Rios, and H. Cheng. 2004. The quantal nature of Ca^{2+} sparks and in situ operation of the ryandine receptor array in cardiac cells. *Proc. Natl. Acad. Sci. USA.* 101:3979–3984.

Xu, L., R. Jones, and G. Meissner. 1993. Effects of local anaesthetics on single channel behavior of skeletal muscle calcium release channel. *J. Gen. Physiol.* 101:207–233.

Young, I.S., C.L. Harwood, and L.C. Rome. 2003. Cross-bridge blocker BTS permits the direct measurement of Ca^{2+} pump ATP utilization in skinned toadfish swimbladder muscle fibers. *Am. J. Physiol. Cell Physiol.* 285:C781–C787.

Zhang, Y., G.G. Rodney, and M.F. Schneider. 2005. Effects of azumolene on Ca^{2+} sparks in skeletal muscle fibers. *J. Pharmacol. Exp. Ther.* 314:94–102.

Zhao, F., P. Li, S.R. Chen, C.F. Louis, and B.R. Fruen. 2001. Dantrolene inhibition of ryanodine receptor Ca^{2+} release channels. *J. Biol. Chem.* 276:13810–13816.

Zhao M, S. Hollingworth, S.M. Baylor. 1996. Properties of tri- and tetracarboxylate Ca^{2+} indicators in frog skeletal muscle fibers. *Biophys J.* 70:896–916.